UNIVERSITY OF AGDER

ENE-500 Master's Thesis

Comparison of ideal solar cell concepts using infield data

by

Tor Gunnar Finnerud

Supervisor:
Rune Strandberg

This master's thesis is carried out as a part of the education at the University of Agder and is therefore approved as a part of this education. However, this does not imply that the University answers for the methods that are used or the conclusions that are drawn.

University of Agder, 2017
Faculty of Technology and Science
Department of Engineering

Abstract

The work done in this thesis has been focused on the comparison of the power production in the ideal single junction cell, intermediate band solar cell, the unconstrained tandem cell, and the area de-coupled 2-terminal constrained tandem cell, using different band gaps. The efficiency and production for each of the concepts have been calculated based mathematical framework previously established, using temperature and irradiation data collected from Kjøita in Kristiansand, using MatLab. The monthly and annual power production for each of the concepts has been calculated and compared. It has been found that the intermediate band solar cell with a band gap optimized for the Am1.5 spectrum, has an annual production 3.6% and 3% higher than the 2-terminal and 4-terminal double junction solar cells with band gaps optimized for Am1.5. Also, the intermediate band solar, 2-terminal and 4-terminal double was shown to have an annual production 29%, 26.5%, and 26.8% higher, respectively, than the single junction cell with Am1.5 optimized band gap.

Preface

I would like to thank my supervisor, Associate Professor Rune Strandberg For his invaluable support during this semester, for finding time to answer questions, and guidance through this thesis.

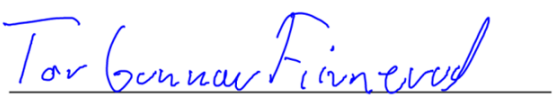

Tor Gunnar Finnerud
University of Agder
Grimstad
June 1, 2018

Individual declaration

The individual student or group of students is responsible for the use of legal tools, guidelines for using these and rules on source usage. The statement will make the students aware of their responsibilities and the consequences of cheating. Missing statement does not release students from their responsibility.

1.	I hereby declare that my thesis is my own work and that I have not used any other sources or have received any other help than mentioned in the thesis.	☑
2.	I further declare that this thesis: - not been used for another exam at another department/university/university college in Norway or abroad; - does not refer to the work of others without it being stated; - does not refer to own previous work without it being stated; - have all the references given in the literature list; - is not a copy, duplicate or copy of another's work or manuscript.	☑
3.	I am aware that violation of the above is regarded as cheating and may result in cancellation of exams and exclusion from universities and colleges in Norway, see Universitets- og høgskoleloven §§4-7 og 4-8 og Forskrift om eksamen §§ 31.	☑
4.	I am aware that all submitted theses may be checked for plagiarism.	☑
5.	I am aware that the University of Agder will deal with all cases where there is suspicion of cheating according to the university's guidelines for dealing with cases of cheating.	☑
6.	I have incorporated the rules and guidelines in the use of sources and references on the library's web pages.	☑

Publishing Agreement

Authorization for electronic publishing of the thesis. Author(s) have copyrights of the thesis. This means, among other things, the exclusive right to make the work available to the general public (Åndsverkloven. §2). All theses that fulfill the criteria will be registered and published in Brage Aura and on UiA's web pages with author's approval. Theses that are not public or are confidential will not be published.	
I hereby give the University of Agder a free right to make the task available for electronic publishing:	YES ☑ NO ☐
Is the thesis confidential? (confidential agreement must be completed)	YES ☐ NO ☑
- If yes: Can the thesis be published when the confidentiality period is over?	YES ☐ NO ☐
Is the task except for public disclosure? (contains confidential information. see Offl. §13/Fvl. §13)	YES ☐ NO ☑

Contents

List of Figures

List of Tables

List of Symbols

Abbreviations

2T	2-Terminal
4T	4-Terminal
Am	Airmass
Decl	Declination
EoT	Equation of Time
IBSC	Intermediate Band Solar Cell
Lat	Lattitude
MPR	Module Performance Rating
PV	Photovoltaic
SJC	Single Junction Cell
STC	Standard Test Conditions
Tst	True Solar Time

Symbols

c	Speed of light
E	Photon Energy
G	Generation
h	Planck constant
I	Current
J	Current density
k	Boltzmann constant
m	Mass
m	Topp cells
n	Bottom cells
P	Power
q	Elemental charge
R	Recombination
R_0	Recombination parameter
T	Temperature
V	Voltage
Z	Zenith angle
EoT	Equation of Time
min	Minutes
s	Seconds
ϵ	Quasi-Fermi energy
Y	Fraction of the year

1 Introduction

Fossil fuels is the main and a finite source of energy in today's market[1]. In 2014 the global coal consumption was 2.93 GTOE(Gigatonnes oil equivalent) and was increasing at a rate of 103 MTOE/year. The oil consumption for the same year was 92.73 million barrels per day(MBD), and the yearly increase was at 1.4MBD. And the global gas consumption was 9.30 BCM(billion cubic meter)/day and increased by a rate of 127.4 MCM/day in the same year.

As the world becomes more concerned about the fossil-fuels impact on the climate, and the economical viability changes as the fuel sources becomes depleted. These concerns have lead to an increased interest in renewable energies, particularly solar energy for its abundance as a source and scalability of the installations, from portable panels to solar power plants.

Solar energy can be divided into two categories: solar thermal energy, where electricity or heating are produced from collecting solar energy in the form of heat. The second category is photovoltaics, where electricity is produced directly from the sunlight. Photovoltaics still has a low contribution to the global energy market with only about 1.3% of the installed production, but the contribution from photovoltaics was almost 20% of the increase in global energy production in 2016[2]. Therefore, research is focused on higher efficiency and lower production costs of solar cells.

but the contribution from photovoltaics was almost 20% of the increase in global energy production

The evolution of photovoltaic technologies can be divided into three categories: First generation, which consists mostly of monocrystalline and polycrystalline silicon cells, with an efficiency in the 15-20% range, which are the dominant type of cells on the market. The second generation is mostly known for thin film solar cells that are made of amorphous silicon, Cadmium Telluride, Copper Indium Selenide or Copper Indium Gallium Diselenide. The third generation introduces new concepts with a higher theoretical efficiency limits compared to the single junction limit proposed by Shockley and Queisser[3]. These concepts are among others, the intermediate band and tandem solar cells[4].

With new emerging technologies it is interesting to investigate how well these concepts might function in a Nordic climate. This work will review the theory of the single junction, intermediate band, the 4-terminal tandem and the relatively new approach of area de-coupled 2-terminal tandem cell. A summary of some related work done in the field, and simulations of the cell concepts to compare the efficiency and production, using irradiation and temperature data measured in 2016 at Kjøita, Kristiansand. The mathematical framework used in this work is based on previous work done in the field of intermediate band and tandem cells, and MatLab will be the analysis tool used for the calculations and plotting.

2 Theory

This section describes the different concepts that will be used in this work. These are:

- Conventional Single Junction Cell
- Intermediate Band Solar Cell
- Tandem Solar Cell

The similarities and differences of the working principles of these concepts will be described, as well as the advantages and disadvantages of implementing these. The limiting efficiencies of the different concepts will be calculated by using Shockley and Queisser's [3] principles of detailed balance.

2.1 Detailed balance theory

Proposed by Shockley and Queisser [3], the principles of detailed balance is a technique of calculating the efficiency of photovoltaic(PV) concepts. The most general approach to this technique is to calculate the photon flux absorption in the solar cell and the flux emission, which are related to generation rate and recombination rate respectively.

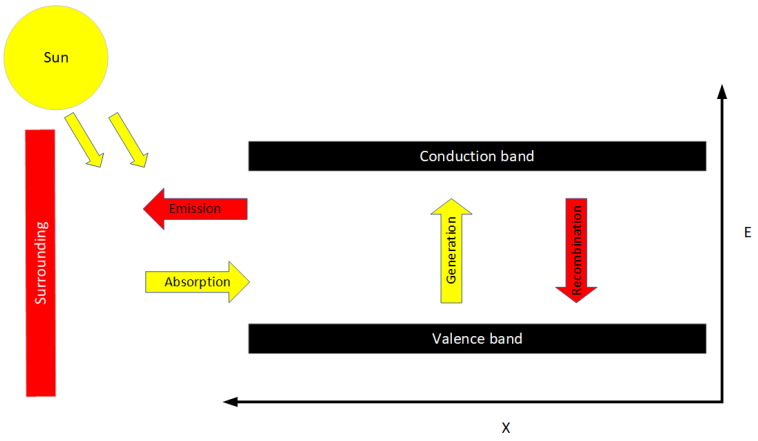

Figure 1: Representation of the detailed balance approximation. Showing generation in yellow and recombination in red. Sunlight is absorbed by the cell and electrons are excited into the conduction. Electrons de-excites back into the valence band and the cell emits photons.

The principle assumes full absorption of photons above the band-gap energy and infinite carrier mobility, allowing collection of carriers independently of where generation occurs in the cell. Also, it assumed that the charge carrier transport is lossless, zero losses from unwanted reflections and a perfect mirror at the back, all recombinations are radiative and one electron is generated for every photon with energy above the band-gap level. Depicted in figure 1, an electron is excited for every photon and recombination emits a photon for every electron that de-excites. Then the solar cell current becomes the difference between generation and recombination multiplied by the elemental charge q.

2.2 Generation flux

The irradiation received by the solar cell can be seen as two different components, direct and diffuse irradiation. The direct component is the irradiation contribution perpendicular to the disc of the sun, this largely varies on factors like cloud coverage, moisture and other atmospheric conditions, shown in figure 2. The diffuse contribution comes from the light scattering in the atmosphere, excluding the direct component. The sum of these components may also be as the global horizontal irradiation[5].

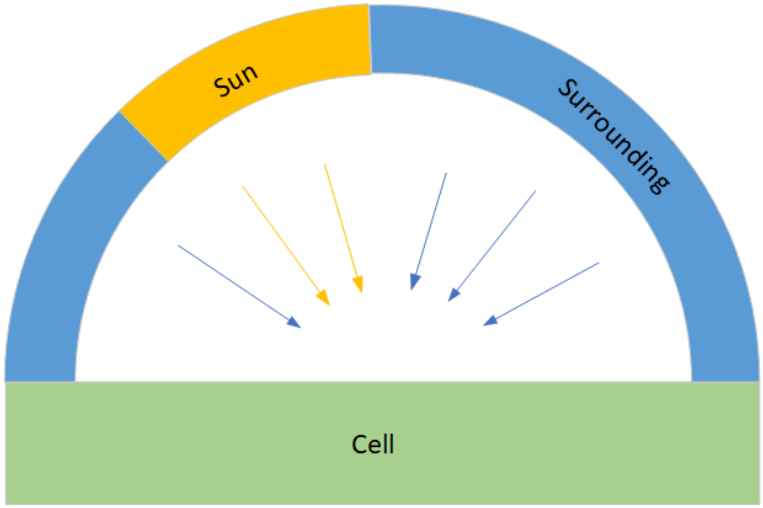

Figure 2: Representation of the surface irradiation, where the yellow parts represent the direct component from the sun and blue the diffuse component form the surroundings and the rest of the sky

Depending on the position of the sun in the sky, the distance the light needs to travel through the atmosphere changes with the sun. When the sun is directly overhead, the distance the light travels corresponds to one atmosphere or Airmass(Am) 1. As the sun descends toward the horizon, the Am increases. The light spectrum's for different Am's is comprised of a range of wavelengths, from infrared to ultra-violet. In each wavelength there are a number of photons, the photon flux is often calculated by summarizing the number of photons in an interval of wavelengths.

2.3 Recombination

Recombination rate of electrons and holes is a process where these carriers annihilate each other, where the electron after one or more steps occupies the hole state. The energy difference between the hole and electron is released during this process. Recombination is divided into three different classes: Radiative recombination, the energy is released in the form of a photon. Non-radiative recombination, the energy is passed on as atomic or molecular vibrations, also known as phonons and auger-recombination, the energy is released in the form of kinetic energy transferred to another electron[6]. The recombination rate is dependant on the separation of the quasi-Fermi levels μ and can be described as[7]

$$\psi_{\text{recombination}}(E_g, \infty, \mu, T_{\text{earth}}) = C \int_{E_g}^{\infty} \frac{E^2}{\exp\frac{E-\mu}{kT_{\text{earth}}} - 1} dE, \tag{1}$$

where C is a constant $C = \frac{2\pi}{h^3 c^2}$, and E_g is the band-gap energy, c is the speed of light, h is the Planck's constant, T_{earth} is the temperature of the earth, k is Boltzmann constant, E is the photon energy.

Fermi-Dirac statistics describes particle distribution over a systems energy states, made up of identical particles that do not occupy the same quantum state in a quantum system, also known as the Pauli

exclusion principle. While the Fermi-Dirac statistics describes the electron and hole population in a material in thermodynamic equilibrium, this changes when excess carrier generation beyond the thermal equilibrium occurs. When a semiconductor material becomes illuminated the majority and minority carriers feature enhanced densities, this requires the Fermi level to shift toward both the valence and conduction band edges. To resolve this the quasi-Fermi concept may be introduced, which allows a way to describe a state of electrochemical non-equilibrium of a semiconductor under illumination. This replaces the Fermi energy ϵ_{F} with quasi-Fermi energies for both the valence ϵ_{Fv} and conduction band ϵ_{Fc}. The quasi-Fermi energy separation then relates to the implied voltage of the illuminated semiconductor by $\epsilon_{\mathrm{Fc}} - \epsilon_{\mathrm{Fv}} = qV$[8].

2.4 Conventional Single Junction Cell(SJC)

The principle of the solar cell is that when sunlight hits the semiconductor material of the cell, an electron gets excited into the conduction band, shown in figure 1, if and only if the energy of the photons of the sunlight is higher than the energy of the band gap in the semiconductor material. However, for photons with higher energy than the band-gap an effect called thermalization becomes a problem. Thermalization occurs when photons with energies larger or much larger than the band-gap excites electron high up in the conduction band. The electron then starts, with high probability, to generate and discharge phonons until its energy is that of the conduction band-edge[9], as shown in figure 3.

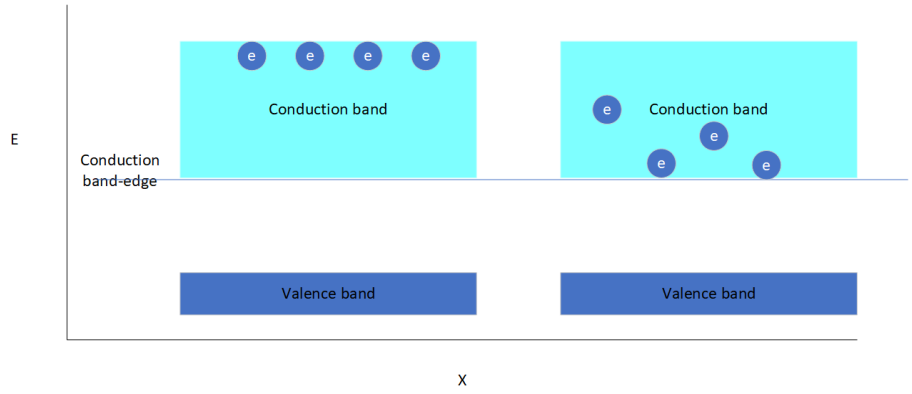

Figure 3: Representation of electrons being excited high up in the conduction band and then settling at the band-edge

According to Shockley and Queisser[3] the highest theoretical efficiency limit in the AM1.5 spectrum and assuming a band gap of 1.34eV was approximately 33.7%.

To model the SJC, as well as the other cells in this work. The principle of detailed balance is applied, which states [3]

$$J = q(G - R), \tag{2}$$

where J is the current density, q the elemental charge constant, G is the photon generation rate, for this work the photon generation is estimated based on standardized spectra and R the recombination rate of the electron hole pairs. The recombination can be calculated using [10]

$$R = C \int_{E_{Gap}}^{E_{Top}} \frac{E^2}{\exp[\frac{(E-qV)]}{kT}] - 1} dE, \tag{3}$$

If $\exp[\frac{(E-qV)}{kT}]$ is much larger than 1, a simplification can be used

$$R = C \int_{E_{\text{Gap}}}^{E_{\text{Top}}} E^2 \mathrm{e}^{\frac{(qV-E)}{kT}} dE, \tag{4}$$

where E_{Top} is the upper band gap limit, usually infinite. V is the cell voltage, and T is the cell temperature.

2.5 Intermediate Band Solar Cell(IBSC)

Thermalization is the largest individual limiting factor of efficiency in solar electrical power. Utilizing the sunlight more efficiently by having additional band-gap interval might increase the cell efficiency, one way of achieving an additional band-gap is the Intermediate band solar cell(IBSC). By adding an intermediate band(IB) in between the conduction and valence band, two photons with energies less than the band gap level should theoretically be able to excite one electron into the conduction band.

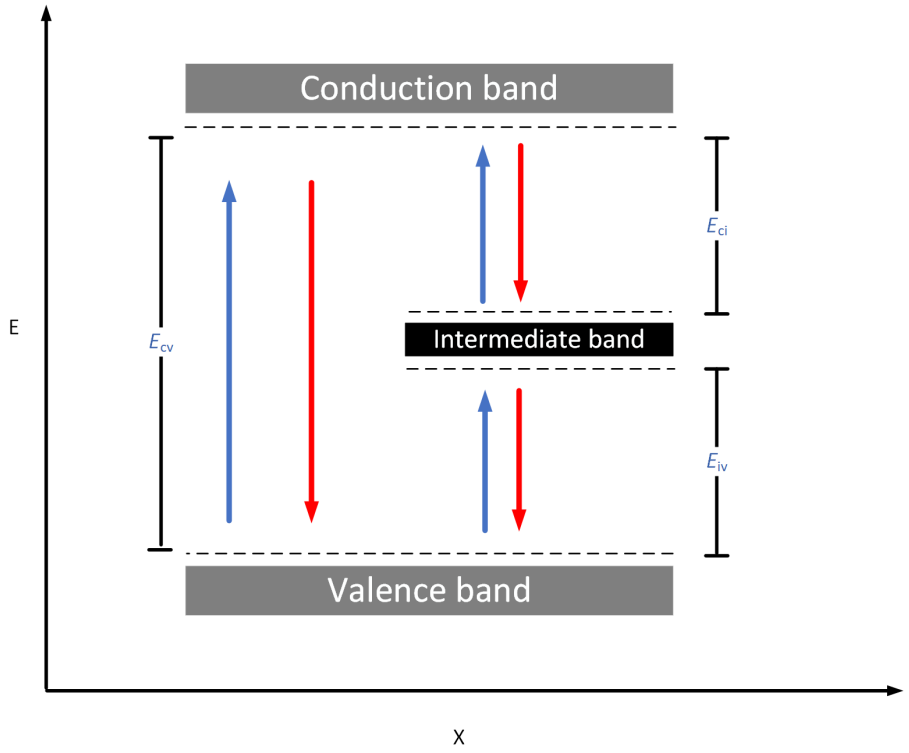

Figure 4: Principal sketch of the Intermediate cell. Where blue arrows are the generation and red arrows are the recombination. Left side electrons are excites over the whole band gap. While on the right side two lower than band gap energy photons, excites an electron into the conduction band.

Figure 4 is a sketch of an IBSC. The intermediate band is currently fabricated by using either quantum dot technology, highly mismatched alloys or with deep impurity bulk materials[11].
R.Strandberg [10] described a mathematical model, which stated

$$J = q(G_{\text{cv}} + 1/2(G_{\text{ci}} + G_{\text{iv}}) - R_{0,\text{cv}} e^{\frac{qV}{kT}} - \frac{1}{2}\sqrt{4R_{0,\text{ci}}R_{0,\text{iv}}e^{\frac{qV}{kT}} + (G_{\text{ci}} - G_{\text{iv}})^2}) \tag{5}$$

where G_{cv} is the generation rate between the valence and conduction, G_{ci} is the generation in conduction-intermediate band and G_{iv} is the generation between the intermediate and the valence band. $R_{,0}$ is the recombination parameters.
The recombinations can be described as

$$R_{0,\text{ci}} = C \int_{E_{\text{ci}}}^{E_{\text{iv}}} E^2 e^{\frac{-E}{kT}} dE \tag{6}$$

$$R_{0,\text{iv}} = C \int_{E_{\text{iv}}}^{E_{\text{cv}}} E^2 e^{\frac{-E}{kT}} dE \tag{7}$$

$$R_{0,\text{cv}} = C \int_{E_{\text{cv}}}^{\infty} E^2 e^{\frac{-E}{kT}} dE \tag{8}$$

Equation 6-8 describes the recombination parameters at the intervals $R_{0.\text{ci}}$ conduction and intermediate band, $R_{0.\text{iv}}$ intermediate and valence band and $R_{0.\text{cv}}$ conduction and valence band respectively.

2.6 Tandem Solar Cell

Tandem solar cells are photovoltaic cells in stacks of two or more. Each of the cells in the stack has a different band-gap, which makes the cells able to use more sunlight more efficiently, thereby increasing the overall efficiency. The cells are configured so that the high energy photons are absorbed in the top cell and the following cells absorb photons with decreasing energy[12].

Figure 5 shows on the left side a 2 terminal(2T) tandem cell, which can either be connected in series or parallel. The right-hand side shows a 4 terminal(4T) cell, i.e., the cells are operated independently of each other. In both cases the high energy photons are absorbed in the top layer cell, and the lower energy photons are absorbed in the bottom layer. The 2T has a drawback in the form of the need to be either current matched, meaning that the current from the top cell and bottom cell needs to be the same, or voltage matched, that the voltage across the top cell and bottom cell needs to be equal. This can reduce the efficiency, especially at times of the day when the infrared parts of the spectrum are dominant. The 4T, on the other hand, do not need matching, but the design complexity increases[13].

The limiting efficiencies under AM 1.5G were investigated by Bremner et al[14]. The efficiencies for constrained 2 terminals (2T), and unconstrained 4 terminal(4T) for a double stack cell configuration is respectively 45.71% and 46.06%.

The mathematical model for the simulations is based on the principle and equations for the 4T and 2T area de-coupled tandem two cell stack configuration [12] [10]. These models assume an ideal cell with perfect back-mirror and low-pass filter between the top and bottom cell, allowing lower energy photons to pass through the top cell into the bottom cell. The 4T configuration can be analyzed as two independent cells, where the output power is,

$$P_{\text{Total}} = P_{\text{Top}} + P_{\text{Bottom}}, \tag{9}$$

where P_{Top} is the power of the top, and P_{Bottom} is for the bottom cell. The current density for each cell is described similarly as for the single junction by

$$J = q(G - R). \tag{10}$$

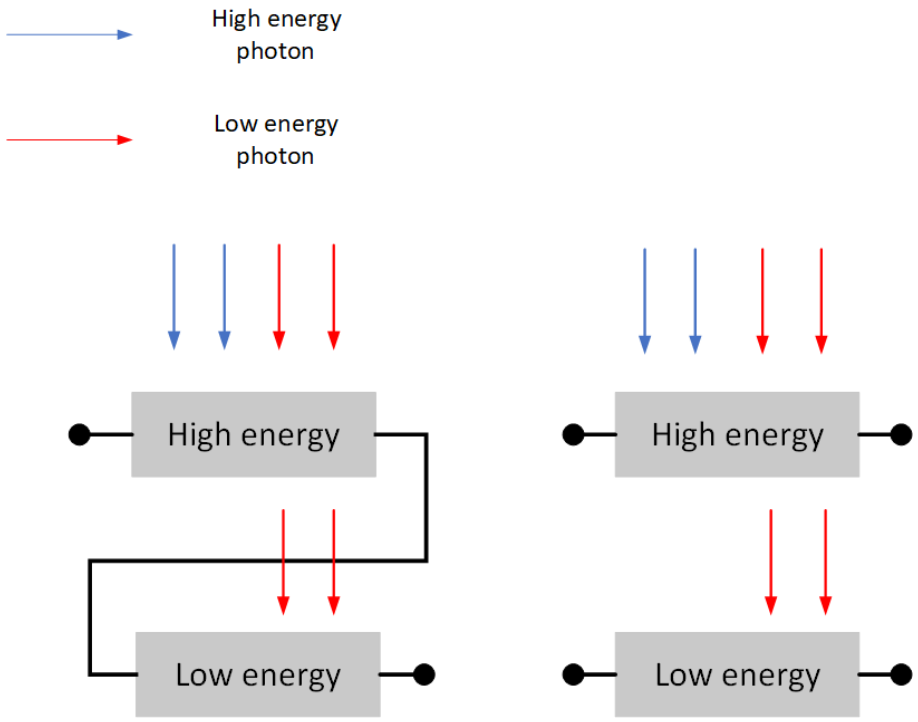

Figure 5: Example sketch of a two cells series connected 2-terminals tandem cell and a independently operated 4-terminal cell. Blue indicate high energy photons and red represents low energy photons

The recombination for the top cell can be described as

$$R_{\text{Top}} = C \int_{E_{\text{Top}}}^{E_{\text{Max}}} E^2 e^{\frac{(qV-E)}{kT}} dE \tag{11}$$

and for the bottom cell as

$$R_{\text{Bottom}} = C \int_{0}^{E_{\text{Top}}} E^2 e^{\frac{(qV-E)}{kT}} dE. \tag{12}$$

A general expression for the power developed for any of the cells can be expressed as

$$P = q(G - R)V. \tag{13}$$

The simulation of the 2T tandem cell is using voltage matching and the method of area de-coupling proposed by Strandberg[12]. By fine-tuning the ratio between "m" top cells and "n" bottom cells(figure6) it is possible to achieve an efficiency equal to that of the 4T tandem cells.

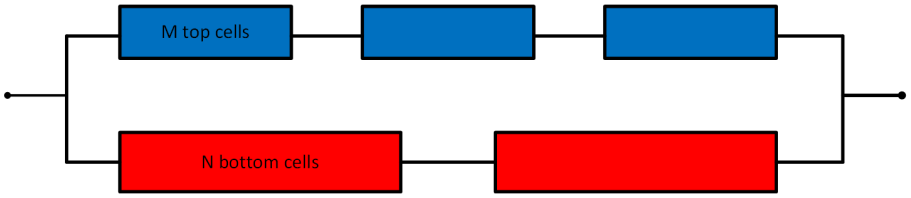

Figure 6: Sketch of a voltage matched 2 terminal tandem cell, with "m" top cells and "n" bottom cells.

With the assumptions mentioned in section 2.1 and and previously in the this section, the current

density for the top cell can be described as

$$I_{\text{Top}} = \frac{qA}{m}(G - (C\int_{E_{\text{Top}}}^{E} E^2 e^{\frac{(qV_{\text{Top}}-E)}{kT}} dE), \tag{14}$$

where I_{Top} is the top cell current and V_{Top} is the cell voltage of the top cell. Similarly the bottom cell becomes

$$I_{\text{Bottom}} = \frac{qA}{m}(G - (C\int_{E_{\text{Bottom}}}^{E_{\text{Top}}} E^2 e^{\frac{(qV_{\text{Bottom}}-E)}{kT}} dE), \tag{15}$$

where I_{Bottom} is the bottom cell current and V_{Bottom} is bottom cell voltage. The power of the 2T tandem cell can then be expressed like

$$P = V(I_{\text{Top}} + I_{\text{Bottom}}) \tag{16}$$

where V is shared voltage across the parallel connection and need to obey the dependency $mV_{\text{Top}} = nV_{\text{Bottom}} = V$. For use in this work, the efficiency at different combinations of "n" and "m" cells for the different band gaps, and can be seen in figures 26-29 in the appendix A.

2.7 Solar position

It is necessary to find an estimate of the suns position throughout the year, in order to know how the AM changes throughout the day for a year. To calculate the solar position these sets of equations collected from the National Oceanic and Atmospheric Administration [15] will be used.
Firstly, the fraction of the year is calculated, which divides the year into a decimal number in radians.

$$Y = \frac{2\pi}{365}\big(d - 1 + \frac{hr - 12}{24}\big) \tag{17}$$

Where Y is the fractional year in radians, d is the day of the year and hr is the hour of the day. With the fractional year its possible to calculate the Equation of Time(EoT), which corrects for the eccentricity of the earth's orbit or the difference between the apparent solar time and the mean solar time, By

$$\begin{aligned} EoT = 229.18\cos(Y) + 0.001868\cos(Y) - 0.032077\sin(Y) \\ -0.01461\cos(2Y) - 0.040849\sin(2Y) \end{aligned} \tag{18}$$

.

Declination angle of the sun(Decl) is the angle between the equator and the sun and can be calculate by,

$$\begin{aligned} Decl = 0.006918 - 0.399912\cos(Y) + 0.070257\sin(Y) - 0.006758\cos(2Y) \\ +0.000907\sin(2Y) - 0.002697\cos(3Y) + 0.00148\sin(3Y). \end{aligned} \tag{19}$$

Where Eot is in minutes and Decl is in radians.
To account variations of the solar time within a certain time-zone, due to longitude variations in a time-zone and can be calculated by

$$Timeoffset = EoT + 4long - 60timezone, \tag{20}$$

where long is the longitude of the desired position, in degrees(East of the prime meridian is in positive), and timezone is the difference from GMT, which is in hours.

$$Tst = hr60 + min + \frac{S}{60} + Timeoffset \tag{21}$$

Where the Tst is the true solar time, the passage of time of the movement of the sun when observed from the earth. in minutes, min is minutes of the hour and sec is the seconds. The hour angle is the conversion of the suns movement in solar time to angles in degrees and can be calculated like

$$Ha = \frac{Tst}{4} - 180 \tag{22}$$

where Ha is the solar hour angle, in degrees. With the previous equations, the zenith angle can now be calculated as a function of Ha, lattitude(in degrees) and Decl, by

$$Z = \cos^{-1}(\sin(Lat)\sin(Decl) + \cos(Lat)\cos(Decl)\cos(Ha)) \tag{23}$$

Where Z is the zenith angle and Lat is the lattitude.

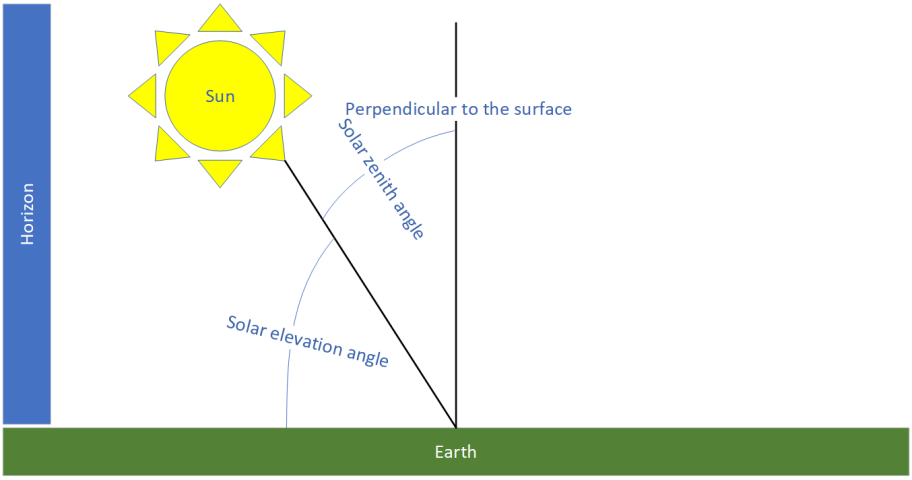

Figure 7: Sketch of solar zenith angle and elevation angle in relation to the surface and horizon

In Figure7 the correlation between zenith and solar elevation angle, where the AM is 1 when the sun is perpendicular to the surface and increases the further it travels toward the horizon.
With the zenith angle the corresponding Am can be calculated using [16]

$$Am = \frac{1}{\cos(Z)} \tag{24}$$

2.8 Band Gaps

$CH_3NH_3PbI_3$ Perovskite has recently been shown to be a highly promising semiconductor material, due to its high power conversion potential with a theoretical efficiency limit of 31%, using the $CH_3NH_3PbI_3$ alloy [17]. As well as high efficiency, it is also attractive because of its relatively low manufacturing cost, its ability for band-gap tailoring, reshape-ability and bend-ability [18].

Silicon(Si) semiconductors are the most established and used technology in the market, and therefore an interesting comparison to make. Using silicon in the subcell in tandem cells has also shown to be promising [19]. Band gap energy for silicon is usually 1.11 eV [20].

Gallium arsenide(GaAs) is a highly relevant comparison due to it having the highest recorded efficiency of an unconcentrated single junction cell, although being very expensive[21]. As a semiconductor material for solar power uses GaAs is good because of its low-temperature coefficient, good low light performance, high efficiency, light and flexible and UV, radiation and moisture resistant[22].

Due to high absorptivity, band-gap tailoring and cost-effectiveness, perovskite-perovskite tandem cells is an exciting material combination to compare [23]. Band-gap values used is 2.25 eV and 1.55 eV for the top and bottom cells respectively. Perovskite and CIGS is another relatively recent combination which might result in low-cost tandem [24]. [25] et al. proposed an AlGaAs/Si combination in an attempt to produce a low cost, high-efficiency tandem cell.

Perovskite/Si is at the moment the most promising contender for reaching the theoretical limit for a two stack tandem cell proposed by D.Vos[26]. Duong et al[27] demonstrated a perovskite/Si tandem cell with an efficiency of 26.4%.

3 State of the art

Solar cell technologies have greatly evolved the last 80 years since the first solar cell reported in 1941 with an efficiency of 1%[28]. This section will take a look at some of the work that has been done in the field.

3.1 Single Junction Cell

Even though a lot of research solar cell technology has shifted towards alternative concepts of reaching an increased utilization of solar power, like multi-junction cells, some strides have been to reach this limit. Silverman et al[29] demonstrated the performance of a GaAs thin film cell, which reached 28.8% efficiency under AM1.5G illumination.

3.2 Intermediate band

One of the major problems with the intermediate-band approach to increase the efficiency of solar cells is the inherent duality nature of the intermediate band in the form of the maximum carrier occupancy. Too low and the transition from IB to CB gets reduced, and if it is too high the transition from VB to IB gets reduced [30]. Research has been commonly done in quantum dot[31], highly mismatched alloys[32], deep impurity bulk materials[33] and now emerging ratchet bands(RB)[34]. The introduction of the ratchet band is to increase the lifespan of the intermediate state thus increasing the efficiency, provided that the RB not be coupled radiatively to the VB[34].

Naitoh et al. presented an efficiency estimation for three-junction 2T and intermediate cells in Japan [35]. It was done by using the detailed-balance on irradiation data over two years, taking into account cell temperature and wind speed. Band gaps were optimized to Am1.5 and 300K. It was concluded that the IBSC is more robust for spectral changes compared to the three-junction cells, especially in shorter wavelength light. Overall the IBSC had about 1% higher production than the 2T three-junction cell, and it was suggested that IBSC would perform well at different locations around the world.

3.3 Tandem Cells

D.Vos [26] proposed a detailed balance limit for Tandem cells. Where it was shown that the efficiency limit for a single cell, double, triple and quad cells were respectively 30%, 42%, 49% and 53%, illuminated by Am1.5. It shows the feasibility of high power density cells for specific applications. The cells are usually connected either in 2T or 4T configuration. 2T in series connection requires current matching that reduce efficiency at certain wavelengths and 4T increases the complexity of the cell. Brown et al. [36] proposed an efficiency limit of 2T current-constrained stacks and found that the relative difference in current between the unconstrained and constrained was 1.5%, for stacks higher than ten the efficiency difference reduced. Bremner et al. [14] presented a similar work where 1-8 cell stack constrained and unconstrained were compared, eight stacks showed the largest efficiency difference with 62.34% unconstrained to 61.42% constrained. As a possible method of increasing the efficiency of 2T tandem stacks, R.Sandberg [12] presented an analysis of area decoupled modules. By independently varying the number of "m" top cells and "n" bottom cells, making it possible to set the voltage/current match with a higher degree of freedom, figure 8.

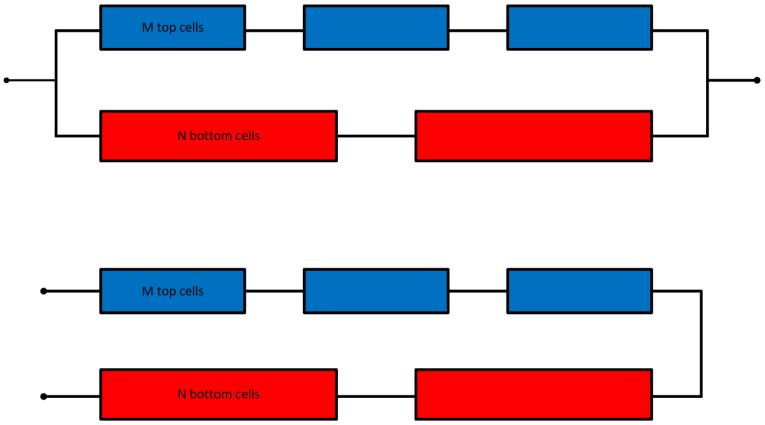

Figure 8: Illustration of the connection configuration for voltage and current matched 2T tandem cell with m - top-cells and n - bottom-cells. The upper configuration shows the voltage matched and the lower shows the current matched. [12]

Jain et al[37] demonstrated a high efficiency double stack tandem cells under Am1.5 illumination, consisting of 1.7 eV GaInAsp top-junction with a 1.1 eV GaInAs bottom junction. This cell bandgap combination had a conversion efficiency of $32.6 \pm 1.4\%$ In a study presented in 2018 by Dupree et al. [38], an efficiency comparison between Standard Test Conditions(STC) and a field test located in Denver was performed. The concepts used were the single junction cell and a 2T and 4T tandem cells. The findings of STC versus In Field(IF) tests were, SJC had $27\%_{\mathrm{STC}}$ and $26.1\%_{\mathrm{IF}}$, the 4T $35\%_{\mathrm{STC}}$ and $34.5\%_{\mathrm{IF}}$, and 2T $35\%_{\mathrm{STC}}$ and $33.8\%_{\mathrm{IF}}$. The current mismatching causes the 0.7% efficiency difference between 4T and 2T. It was also found that the temperature properties of the perovskite compensated for the losses due to current mismatch. The temperature properties of perovskite are the opposite of many semiconductor materials in the way that the band-gap widens, i.e., the needed energy increases as the temperature rises, unlike c-Si that narrows. In effect, as the sun rises and the irradiance and temperature increases, the current in the c-Si bottom cell increases relative to the perovskite top cell, and this counteracts the losses caused by the spectral miss-match. This occurs only when just one of the tandem-subcells is perovskite[38].

3.4 Spectrum

In a study conducted by Schweiger et al[39], it was investigated how different climates impact the performance of photovoltaic modules. The modules used in the investigation was placed in Germany, Italy, India, and Arizona(USA), thereby covering four different climate zones. Influences on the performance that were taken into consideration were module temperature, low irradiation, soiling, angular and spectral effects. What they found was figure 9 a large spread in performance, up to 23% module

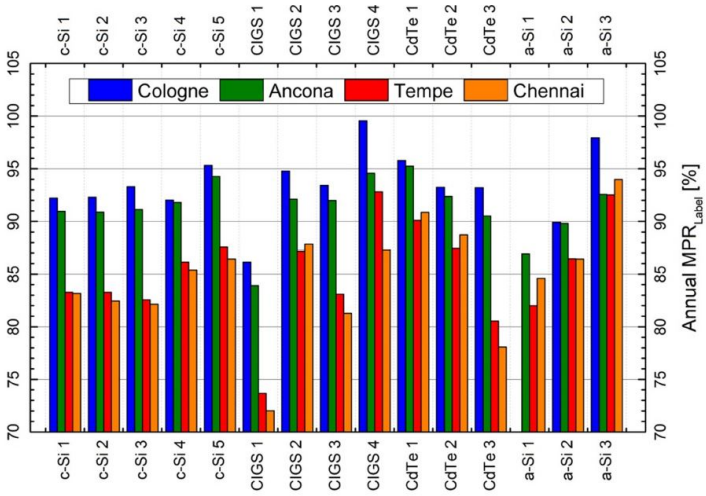

Figure 9: Module performance ration of the different modules at each location.(Collected from[39])

performance ratio(MPR) difference. The highest variations between small and largest MPR in the different locations was, 23% in India, 21% in Arizona, 14% in Germany and 12% in Italy. The differences caused by climate are the most significant between India and Germany of 5-7%, with the occasional observation of 14%.

Liu et al. [40] investigated how spectral variation, low irradiance, and temperature would affect the performance ratio of a single junction, 2T tandem and 4T tandem, with an array of different band-gaps. In the locations of Denver, Colorado, and Singapore.

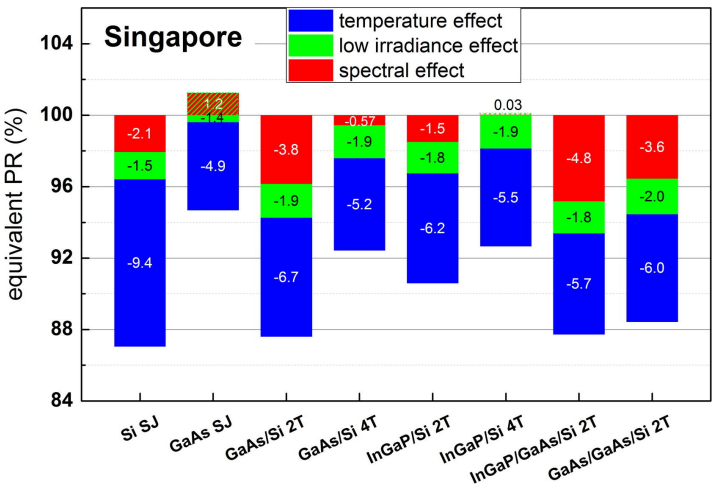

(a) Loss contributions in Singapore. Major temperature and spectral losses contributing to the reduction in efficiency. Collected from[40]

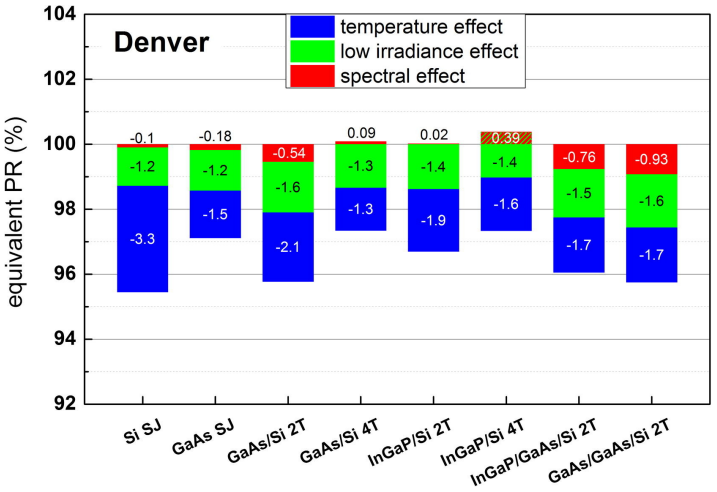

(b) Loss contributions in Denver. Temperature and low irradiance heavily influencing the efficiency reduction, considerably less temperature loss than Singapore. Collected from[40]

The contributions to losses are described in Figure 10a. It was concluded that the spectral losses in tropical climates could be considerable for 2T tandem cells, while small for 4T cells and it was suggested that the 4T tandem cells with optimal sub-cells are the most promising concept to replace the single junction cells. It was predicted that temperature would influence the tandem cell less compared to the single junction cells, which figure 10a corroborate.

Kvifte et al[41] performed a study on the spectral distribution in the Nordic countries. The spectral distribution they found for Tromsø and Aas is given in table 1.

Table 1: Table shows the spectral distributions for Aas and Tromsø, with percentage(%) of sunlight with photon energy(Ev) for each of the locations

Photon energy(eV)	Aas(Percentage of incident light with photon energy)(%)	Tromsø(Percentage of incident light with photon energy)(%)
3.22-4.2eV	13.3-14.5%	13.4-15.2%
1.97-2.5eV	19-20.6%	19.8-21.7%
1.79-1.97eV	13.6-16.7%	9.9-11.9%
0.44-1.79eV	43.7-49.6%	48.3-50.1%

4 Simulations

The cell concepts simulations done in Matlab is based on the previous work done by Strandberg[10][12]. The assumptions for the cells have been previously mentioned in section 2.1 and 2.6. Also, it is assumed that using the spectral irradiance for AM 1, 1.5, 2, 3, 5 and 10 gives an adequate representation of the incoming solar energy. Flowcharts have been used to give a simplified view of the MatLab programming.

4.1 Solar position

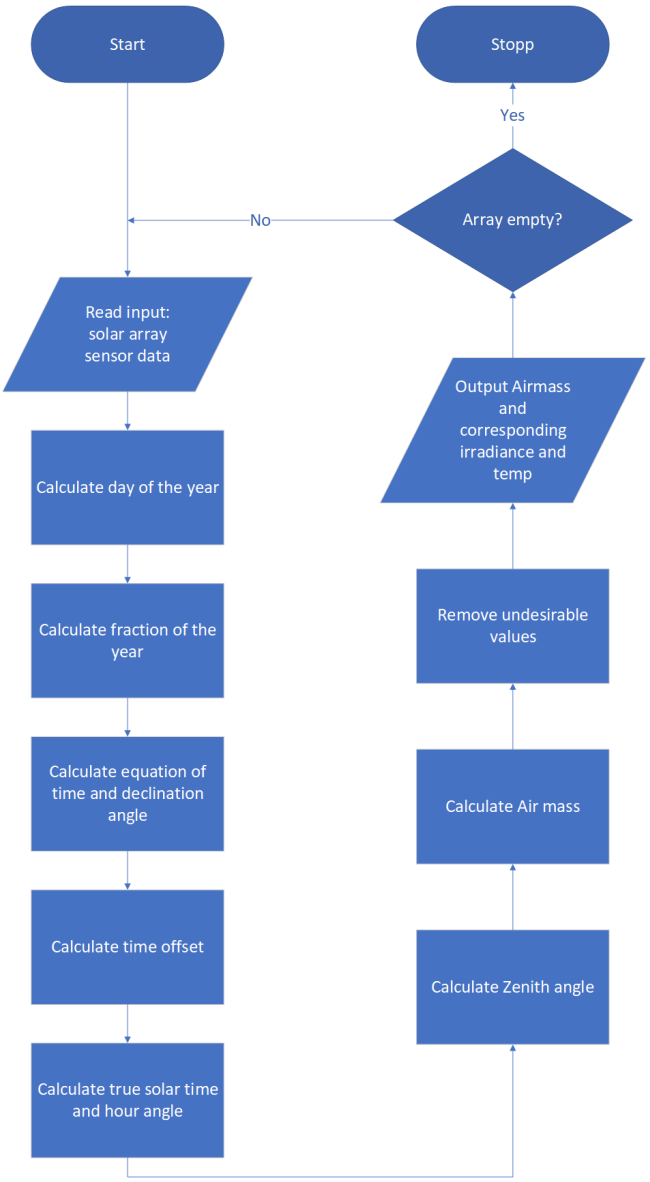

Figure 11: Flow chart for the solar position calculations in matlab

Figure 11 shows the data flow and order of calculations for the suns zenith angle each hour of the day, during the year. Inputs are seconds, minutes, hours, the day of the year, longitude, latitude and time-zone. The end product is the air mass based on the suns position. Values that corresponds to the sun being at the other side of the globe, i.e., night-time, are ignored.

4.2 Spectra

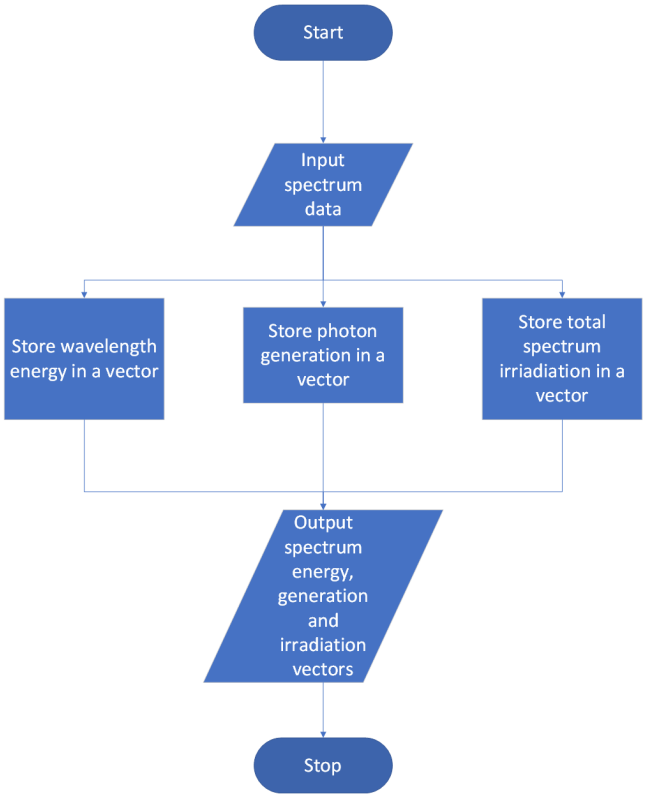

Figure 12: Flow chart of the extraction of spectrum data in matlab. Text files containing the photon energy, irradiance and number of photons for Am 1,1.5,2,3,5 and 10. They are imported and then stored in an array for later use in the concept simulations

The flowchart in figure 12 described the function that imports and store the approximate photon energy in eV, irradiation in W/m^2 and photon generation in $\frac{photons}{m^2 s}$ for the respective spectra, then storing these values in an array. This array is used in the in the concept simulations.

A normalizing factor has been applied to the cell simulations to normalize the calculations with respect to the measured irradiation. This is done by,

$$\frac{P_{\text{measured}}}{P_{\text{tot.irr}}} \tag{25}$$

where P_{measured} is the measured irradiance in W/m^2 and $P_{\text{tot.irr}}$ is the total irradiance in the spectrum, in W/m^2. This ratio is then multiplied with the spectrum's photon generation and total irradiation

4.3 Simulation of concepts

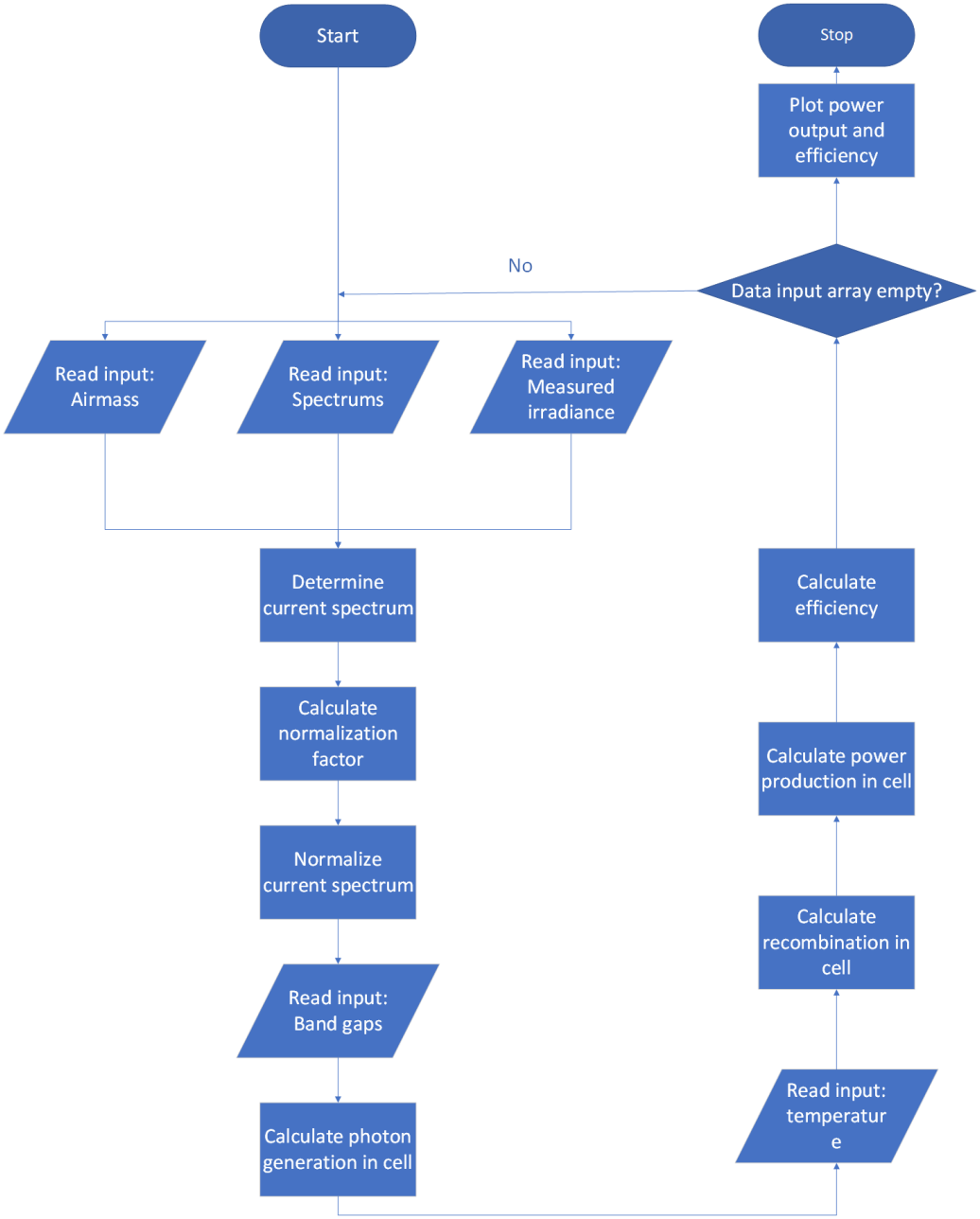

Figure 13: Shows a general sketch of the steps each of the concept simulations undergoes, even if the equations used is not the same ones at each step.

Figure 13 shows the general principle behind the simulations conducted. The calculations done for each of the concepts are repeated for every point of data from the in field measurements. Four different band gaps have been used in each simulation, corresponding to a semiconductor material. Typical for all the concept simulations is that first, the output of the solar position function figure 11 is read, then the amount of photons with above band-gap energies is estimated. Which depends on the Am spectrum the solar position function determines based on the time of day. Then the correction factor equation 25 is applied, and the recombination rate is calculated. The maximum power point P_{mpp} as a function of V_{mpp} is calculated by applying a minimization function to the general equation $P = qV(G - R)$, which is done because the equation only has one maximum point. The efficiency is then calculated based on the power generated and the total irradiation in the current spectrum.

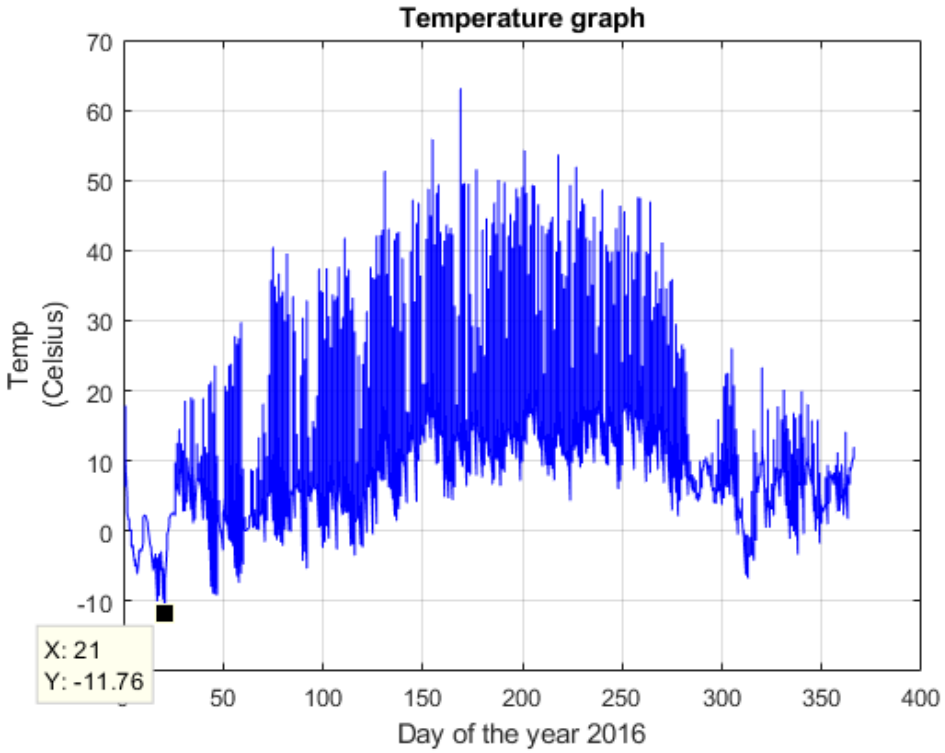

Figure 14: Temperature cell plot for year 2016, used in the simulations for cell temperatures

Figure 14 shows a plot of the cell temperature data that will be used in the simulations. It shows a couple of extra cold temperature occurrences during the winter and a heat peak during the summer, this will likely effect the efficiency of the cells.

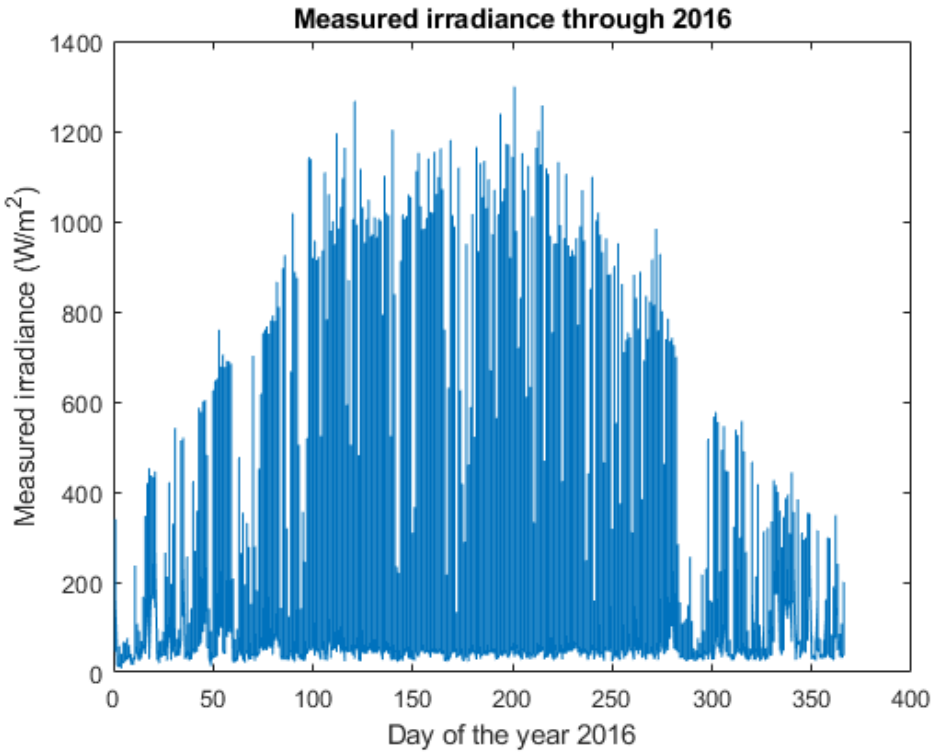

Figure 15: The measured irradiance for the year 2016

Figure 15 shows a plot of the measured irradiance used in the simulations.

5 Results

This section contains the results of the simulations conducted and sorted as:

- Cell concepts power generation and efficiency plots
- Monthly power production comparison
- Power production comparison for the whole year

5.1 Single junction

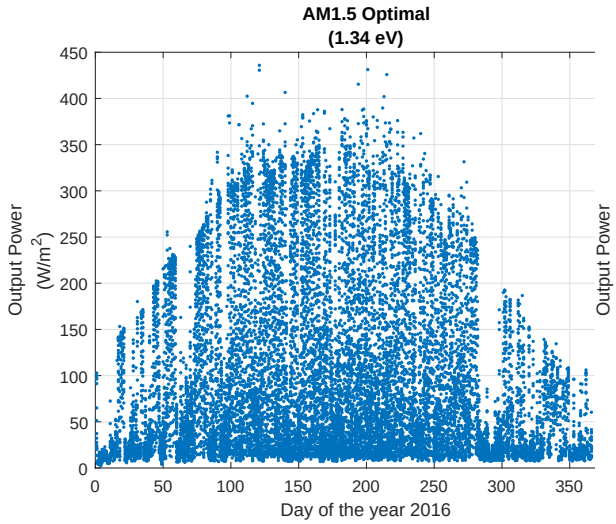

(a) Power generation for the SJC with Am1.5 optimal band gap

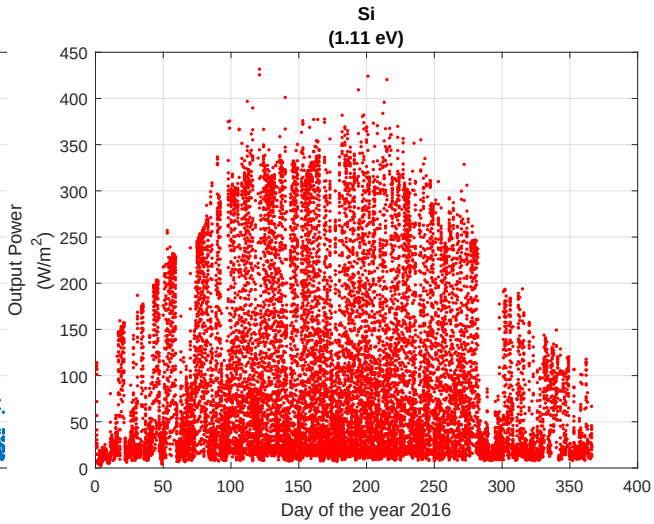

(b) Power generation for the SJC with Si equivalent band gap

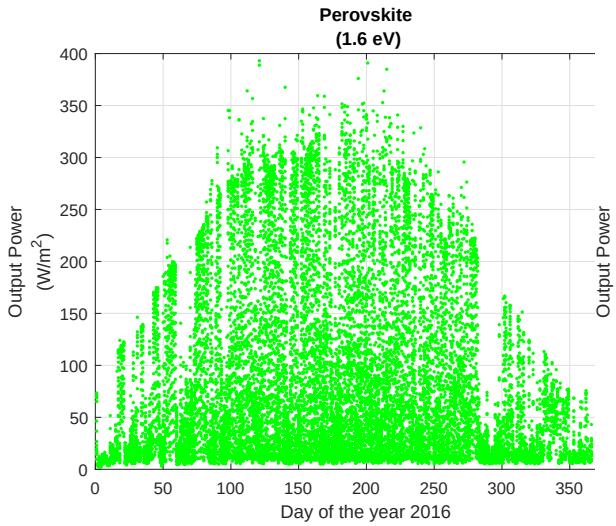

(c) Power generation for the SJC with perovskite equivalent band gap

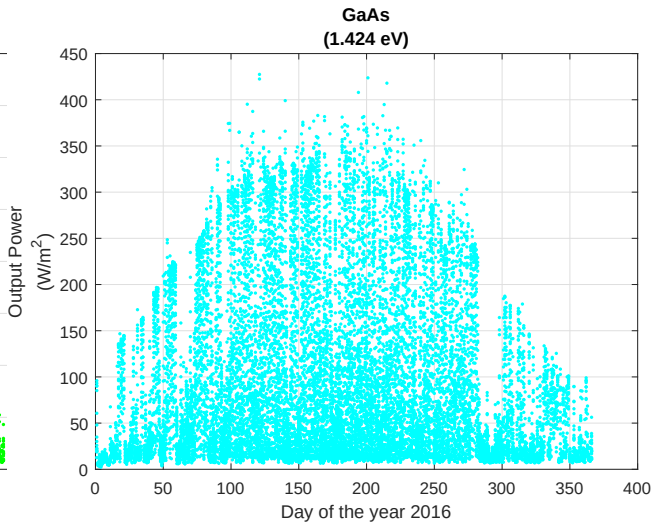

(d) Power generation for the SJC with GaAs equivalent band gap

Figure 16a, 16b,16c and 16d shows power density for SJC simulations for each point of measured data. In common for all four simulations is that it seems the power density is the highest in April and May. Figure 16a, 16b and 16d shows a very similar power generation because the difference in band gap level is relatively small, with an upper-end density in the range of 300-350 W/m^2 in the late spring and summer and peaks up to 450 W/m^2. Power density in 16c is considerably lower than in the three others, caused by the relatively wider band gap.

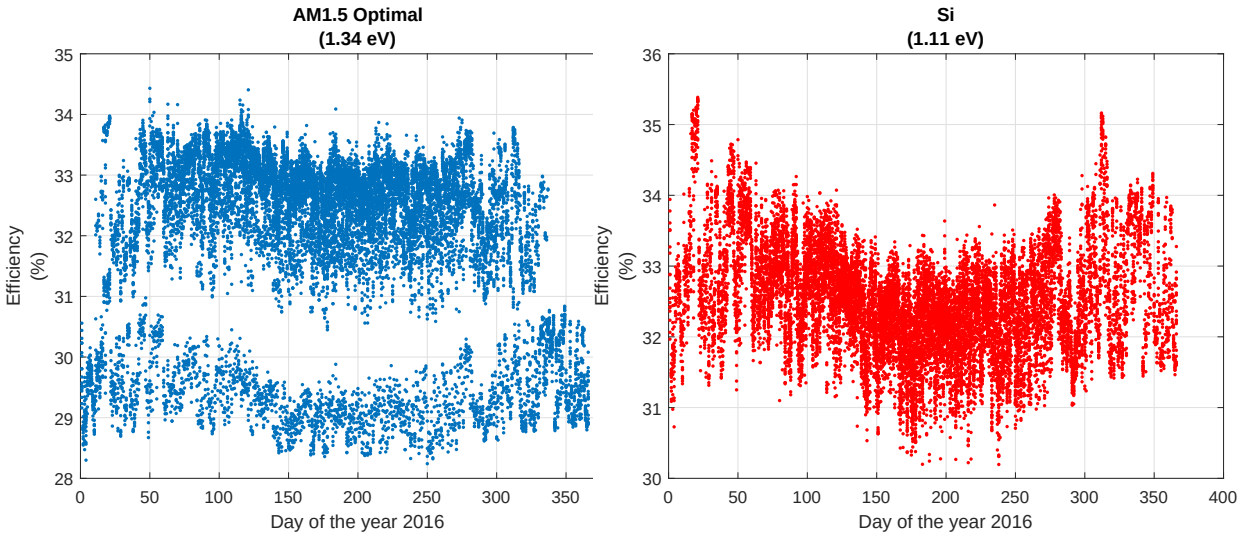

(a) Efficiency of the SJC with Am1.5 optimal band gap

(b) Efficiency of the SJC with Si equivalent band gap

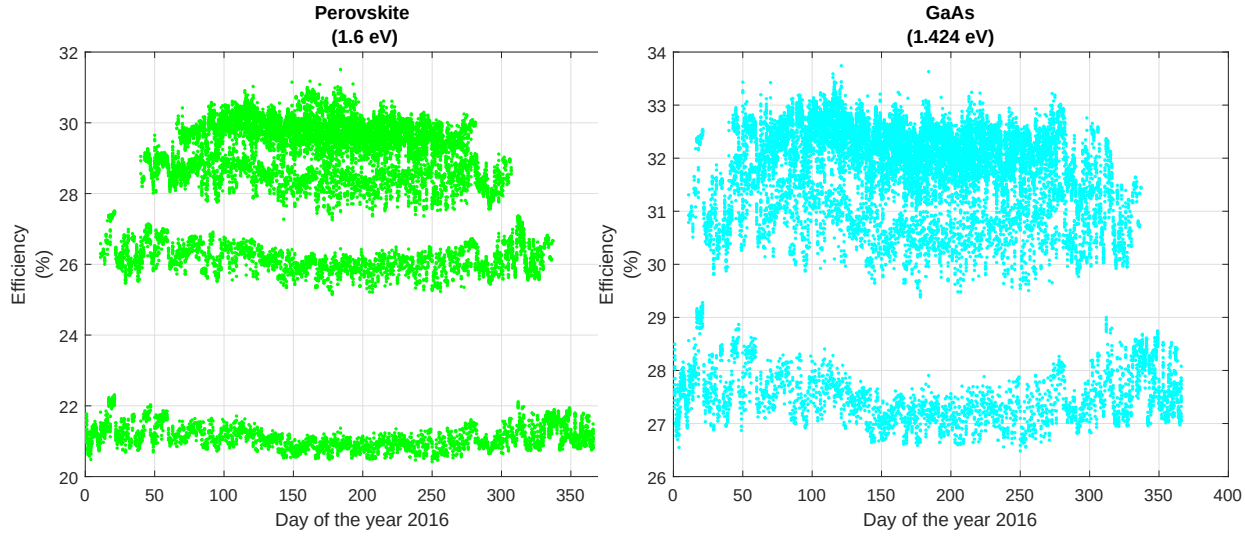

(c) Efficiency of the SJC with perovskite equivalent band gap

(d) Efficiency of the SJC with GaAs equivalent band gap

Figures 17a,17b,17c and 17d shows the efficiency results of the simulations for the SJC at every point of the measured data. Figure 17a seems to have the highest efficiency overall, with up to 33-34% in the spring, summer, and autumn. Figure 17d have the lowest efficiency with just above 31% mid-summer and as low as 21% at times. In figure 17b the most noticeable is the peaks in January and November reaching close to 35.5%. Figure 17d is overall slightly worse than 17a.

5.2 Intermediate band

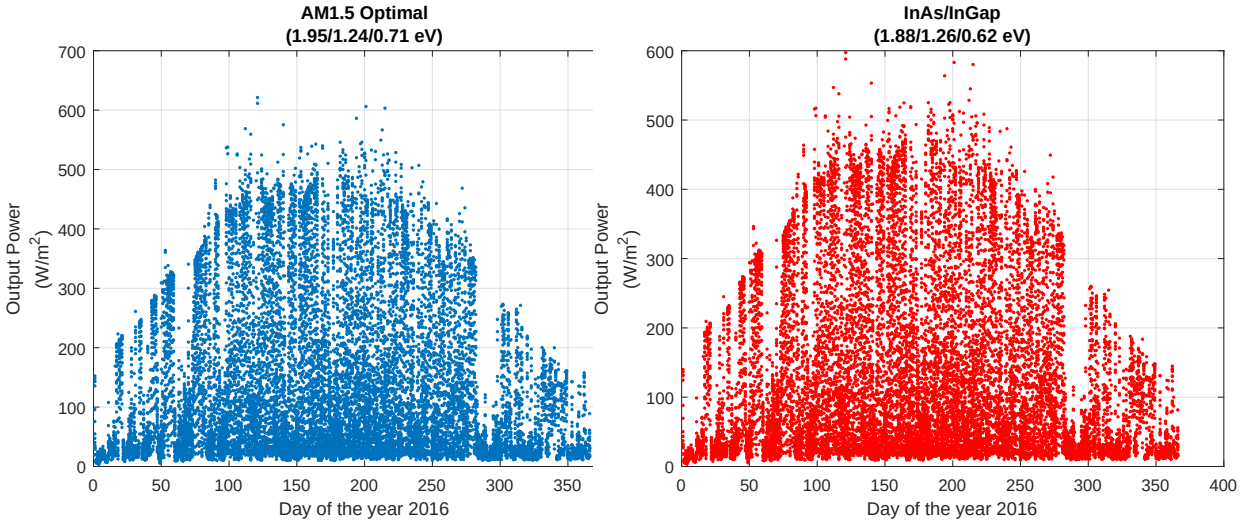

(a) Power generation of the IBSC with Am1.5 optimal band gap

(b) Power generation of the IBSC with InAs/InGap equivalent band gap

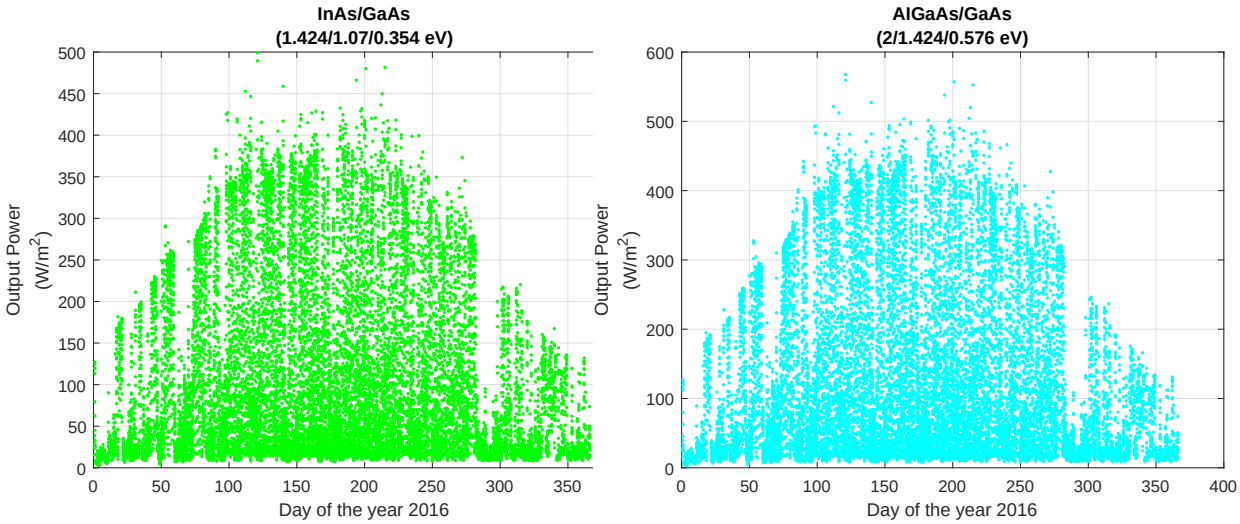

(c) Power generation of the IBSC with InAs/GaAs equivalent band gap

(d) Power generation of the IBSC with AlGaAs/GaAs equivalent band gap

Figures 18a, 18b, 18c and 18d shows power densities for the intermediate band solar cell simulations for every point of measured data. Figure 18a has the overall highest power density throughout the year, with up to 500 W/m^2 in late spring and summer, and some peaks in the 500-600 W/m^2 range. In figure 18c it can be seen that in the late spring and summer the power density reaches around 500 W/m^2, which is the overall lowest power density. Figure 18b and 18d have a lower power density than figure 18a, with a difference around 25-50 W/m^2.

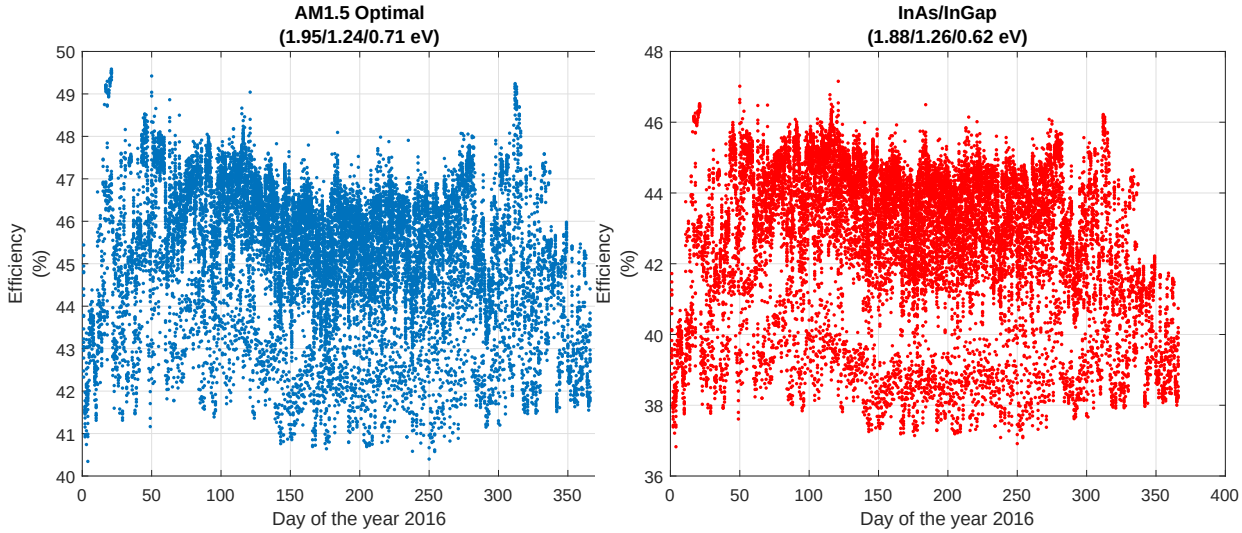

(a) Efficiency of the IBSC with Am1.5 optimal band gap

(b) Efficiency of the IBSC with InAs/InGap equivalent band gap

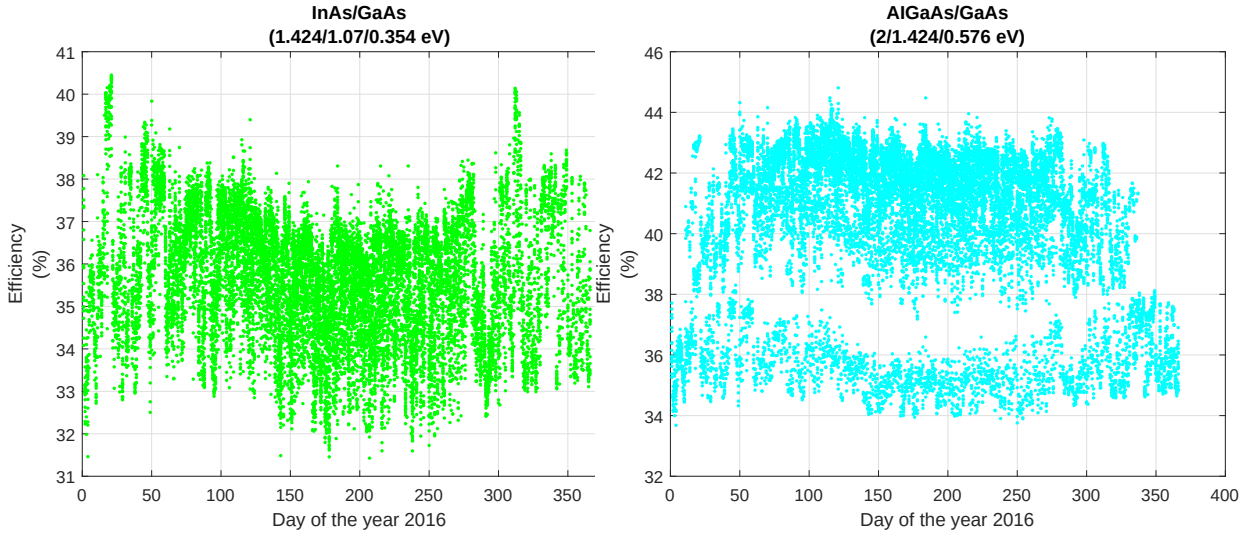

(c) Efficiency of the IBSC with InAs/GaAs equivalent band gap

(d) Efficiency of the IBSC with AlGaAs/GaAs equivalent band gap

Figures 19a, 19b, 19c and 19d shows the efficiency plots for the intermediate band solar cell simulations. Figure 19a has the highest efficiency, largely being in the 45-48% region and noticeably the peaks in January and November reaching 49.5%. Figure 19c has the lowest efficiency, with the highest point being at about 40.5%. Figure 19b do not have as pronounced wintertime peaks as figure 19a and the efficiency is typically around 42-46%. And figure 19d has an efficiency generally 2-4% lower than figure 19b.

5.3 4T tandem cell

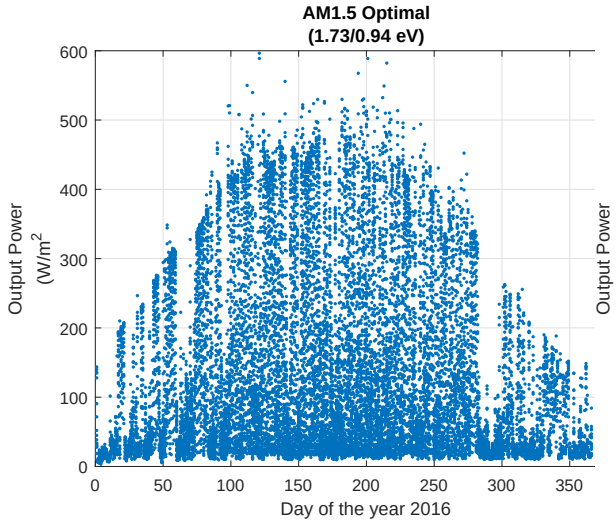

(a) Power generation of the 4T tandem with Am1.5 optimal bandgap

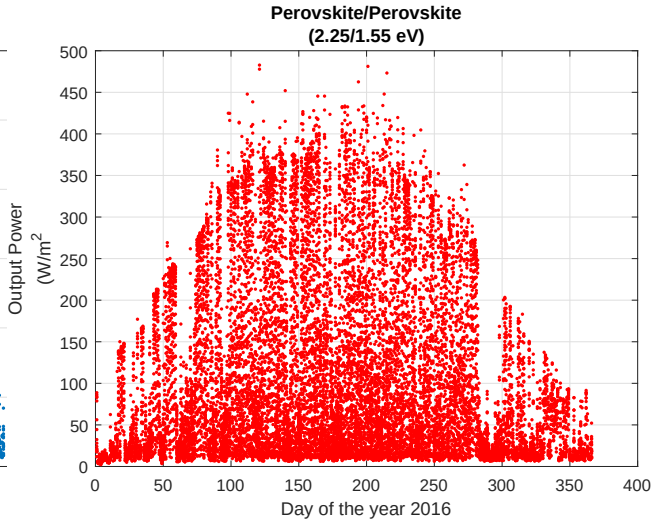

(b) Power generation of the 4T tandem with Perov/Perov equivalent band gap

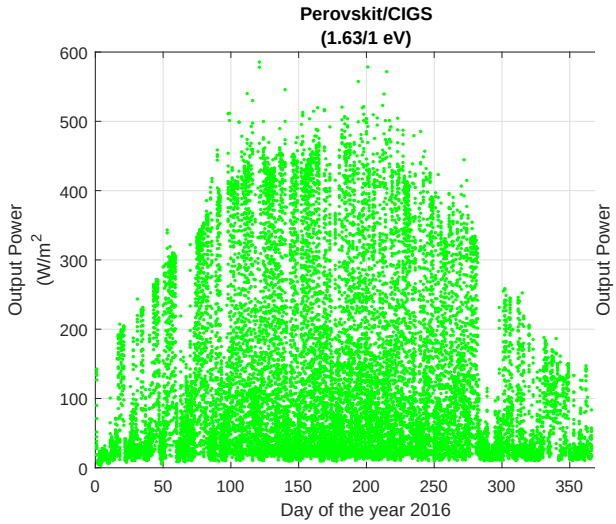

(c) Power generation of the 4T tandem with Perov/CIGS equivalent band gap

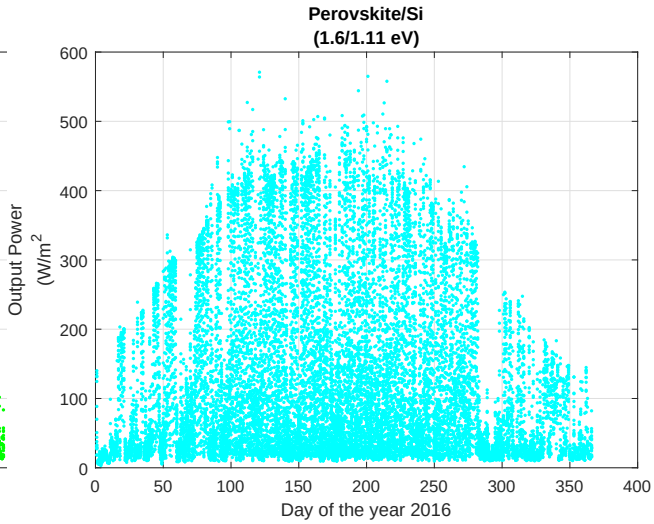

(d) Power generation of the 4T tandem with Perov/Si equivalent band gap

Figures 20a, 20b, 20c and 20d shows power density results of the 4T tandem cells. Figure 20a shows a power density up to about 450 W/m^2 with peaks reaching 600 W/m^2. Figures 20c and 20d shows results very similar to that of figure 20a. While figure 20b seems to about 50-75 W/m^2 lower than figure 20a.

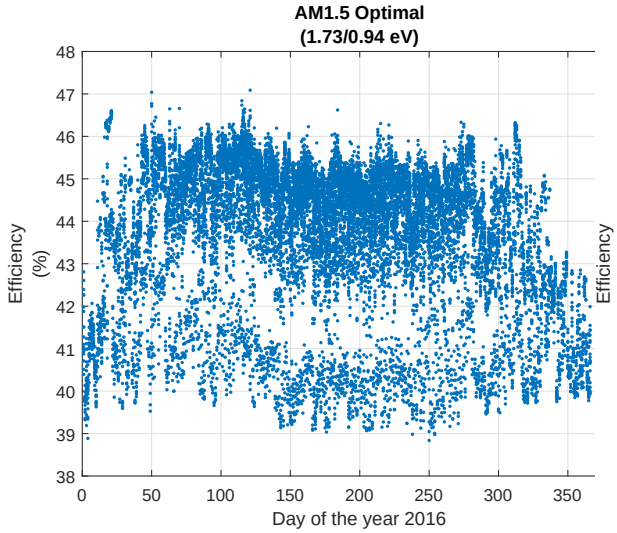

(a) Efficiency of the 4T tandem with Am1.5 optimal band gap

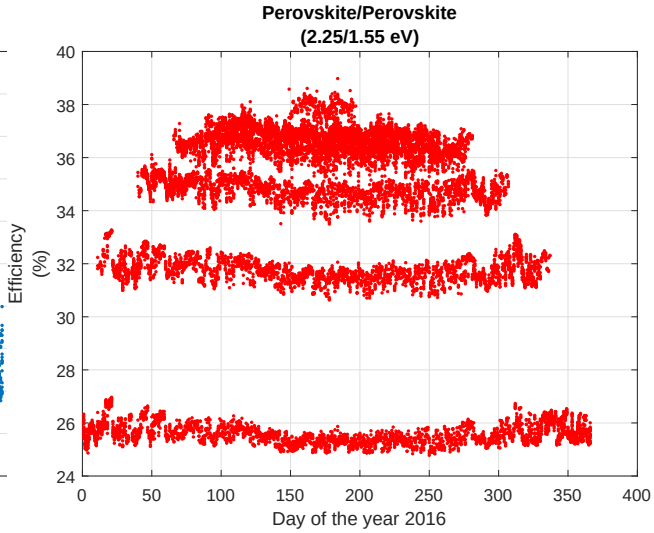

(b) Efficiency of the 4T tandem with Perov/Perov equivalent band gap

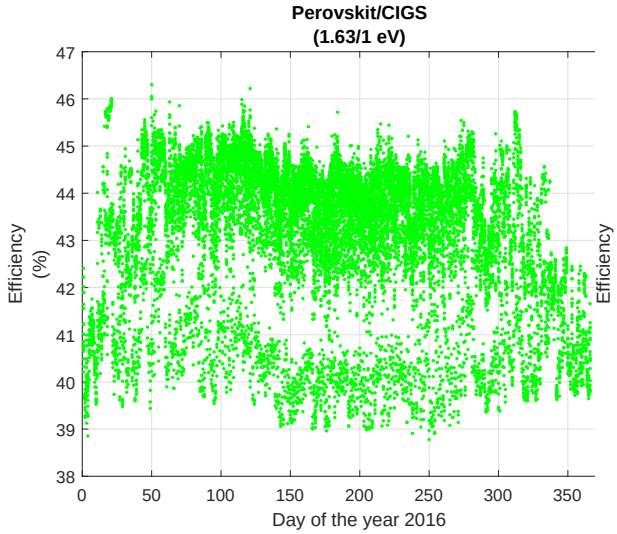

(c) Efficiency of the 4T tandem with Perov/CIGS equivalent band gap

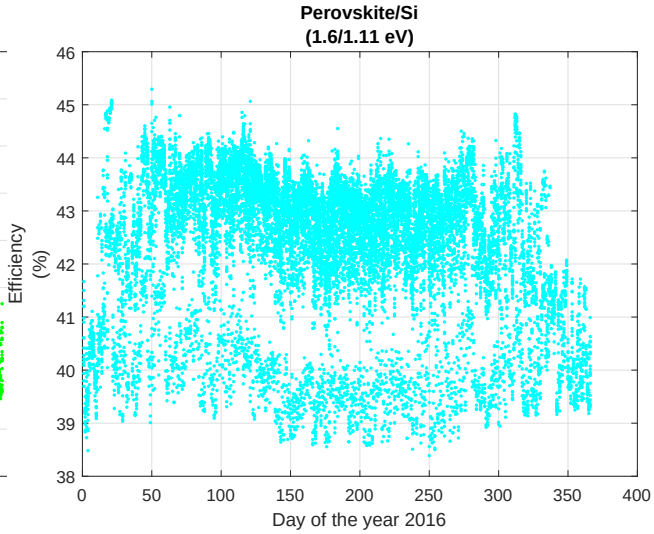

(d) Efficiency of the 4T tandem with Perov/Si equivalent band gap

Figures 21a-21d shows the efficiency results for the simulations of the 4 terminal tandem cells. Unsurprisingly figure 21a has the highest efficiency up to about 46% and some peaks reaching 47%. Figure 21c has a slightly lower overall efficiency compared to 21a, with a difference around 0.5-1%. For the case in figure 21d, it has about 2% lower efficiency compared to figure 21a. Figure 21b has the lowest efficiency with about 38%. Also, a "layered" shape can be observed and will be discussed.

5.4 2T tandem cell

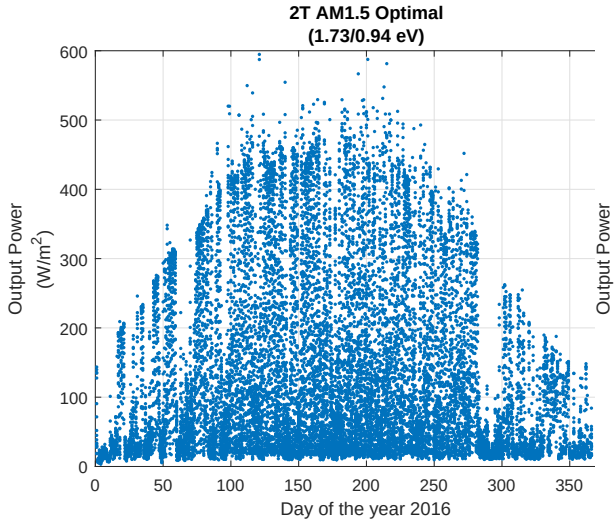

(a) Power generation of the 2T tandem with Am1.5 optimal band gap

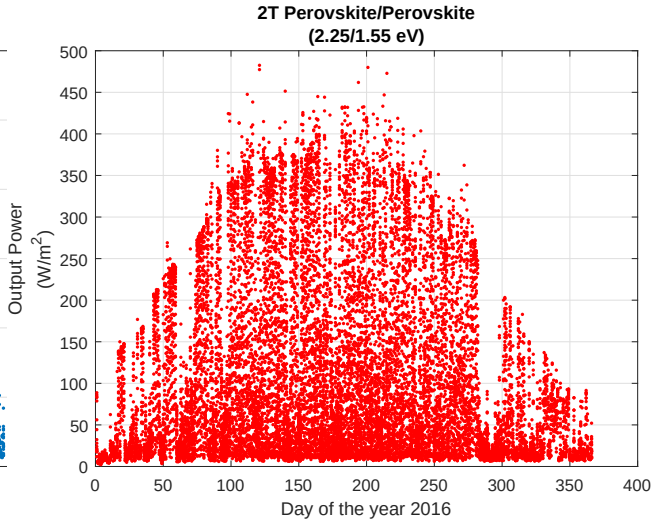

(b) Power generation of the 2T tandem with Perovskite/Perovskite equivalent band gap

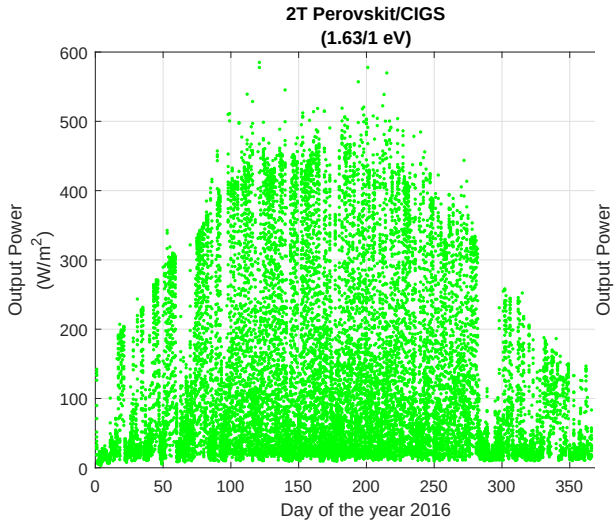

(c) Power generation of the 2T tandem with Perovskite/CIGS equivalent band gap

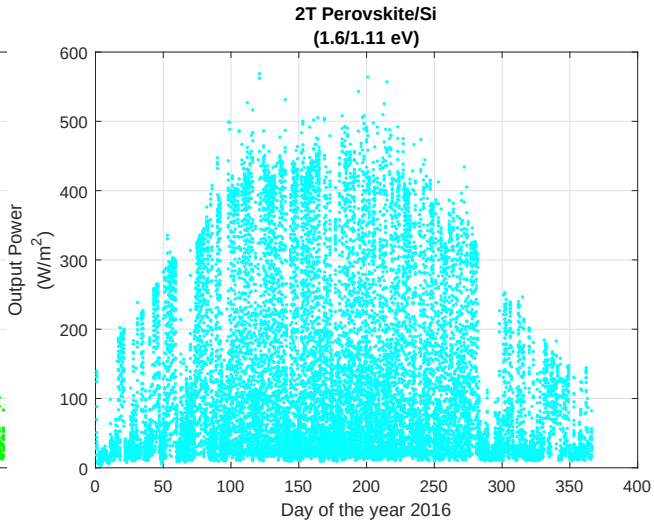

(d) Power generation of the 2T with tandem Perovskite/Si equivalent band gap

Figures 22a-22d shows the power density plot of the simulation of the 2 terminal tandem cell. Figure 22a shows a power density of about 450 W/m^2 and peaks reaching 600 W/m^2. Comparing figures 22c and 22d to figure 22a the difference seems to be small. Figure 22b shows a power density lower than the other three, with a density up to 400 W/m^2 and peaks reaching 500 W/m^2.

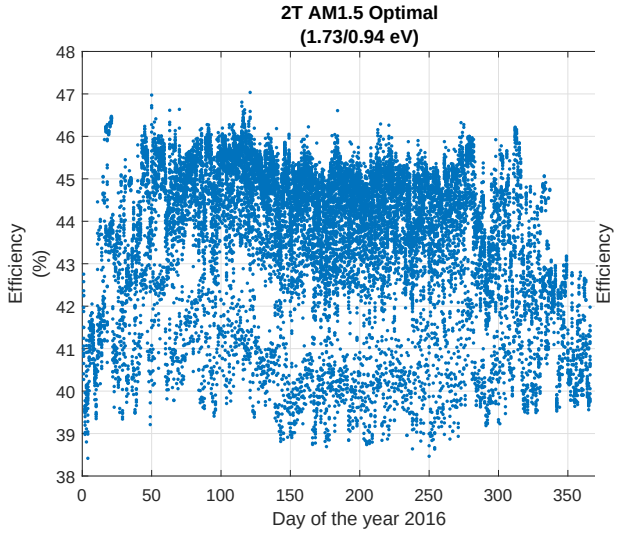

(a) Efficiency of the 2T tandem with Am1.5 optimal band gap

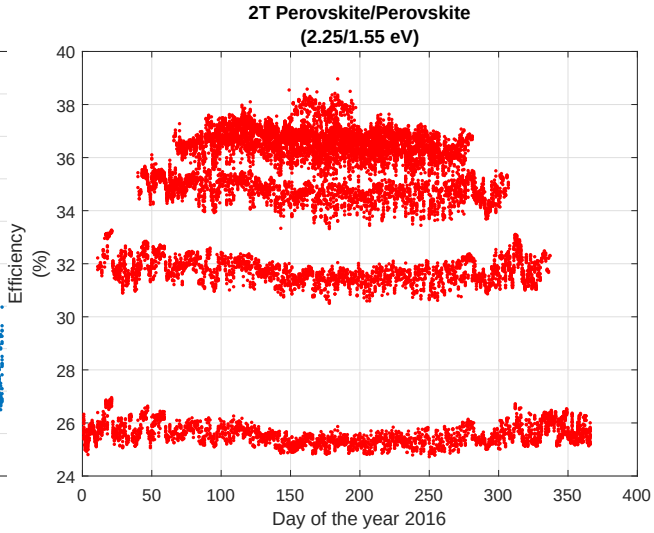

(b) Efficiency of the 2T tandem with Perovskite/Perovskite equivalent band gap

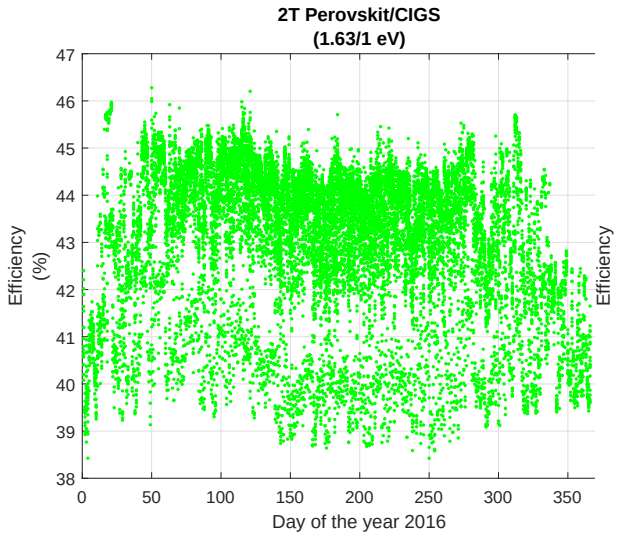

(c) Efficiency of the 2T tandem with Perovskite/-CIGS equivalent band gap

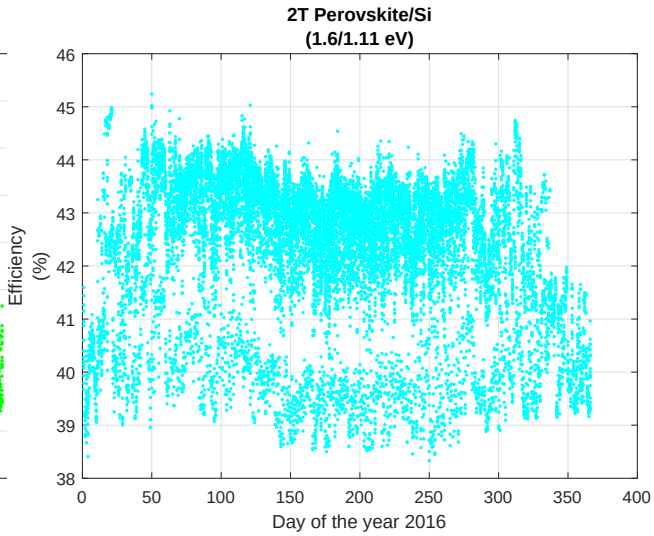

(d) Efficiency of the 2T tandem with Perovskite/Si equivalent band gap

Figures 23a-23d shows the efficiency plots for the 2 terminal tandem cell. Figure 23a has the highest efficiency of these four simulations, with an efficiency up to 46% and peaks reaching 47%. Figures 23c and 23d compared to 23a shows an efficiency difference of about 1% and 2% lower respectively. Figure 23a has the lowest efficiency with about 38% at the highest, the "layered" shape previously mentioned can be observed here as well.

5.5 Production

Figure 24: Showing the production on a per monthly basis for each of the cell concepts

The production on per monthly basis in kWh/m^2 of 2016, for the simulations of the ideal solar cell concepts, with varying band gaps is shown in figure 24. It can be seen that the IBSC with the Am1.5 optimal band gap has the highest monthly production throughout the year. 4T tandem and 2T tandem with the Am1.5 optimal band gap have second and third best monthly production respectively. Unsurprisingly the four SJCs have the lowest monthly production. Interestingly, it can be seen that the IBSC InAs/GaAs cell produces better in the winter, spring and autumn months compared to the 2T perovskite/perovskite tandem cell, but has lower production during the summer. For reference see tables 2 and 3.

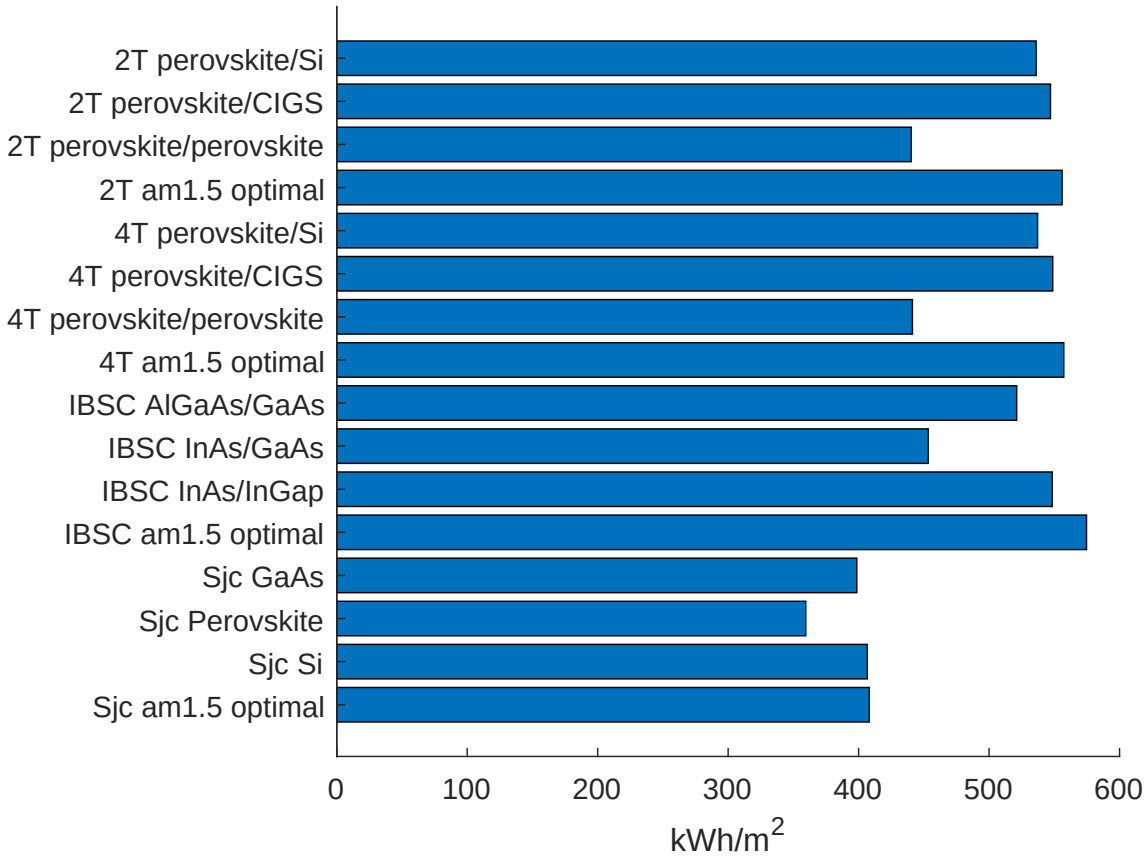

Figure 25: Comparison of the annual power production for 2016, for each of the concepts. The X-axis is the annual kWh/m^2

In figure 25 the comparison of the annual production for the year 2016 for each of the cell concept simulations, is shown. It can be seen that the IBSC with the Am1.5 optimal band gap has highest annual production, with 574 kWh/m^2. The 2T and 4T tandem cells with Am1.5 optimal gap shows a very similar annual production compared to each other, with 554 and 557 kWh/m^2 respectively. It gives the IBSC a 3.6% higher production than the 2T, and a 3% higher production than the 4T. Looking at the 2T and 4T perovskite/CIGS and the InAs/InGap IBSC, it can be seen that these three are almost identical, with 547, 548 and 548 respectively. The 2T and 4T perovskite/Si tandem cells can be seen to have almost identical production as well, at 536 kWh/m^2 for the 2T and 537 kWh/m^2 for 4T. Compared to the IBSC InAs/InGap, the InAs/InGap has a 2% and 2.2% higher annual production than the 4T and 2T perovskite/Si respectively. The SJCs have an annual power production of 408, 406, 359 and 398 kWh/m^2 for the Am1.5 optimal, Si, Perovskite and GaAs respectively. Comparing the SJC Am1.5 optimal and Si to the IBSC and tandem cells with Am1.5 band gaps, the IBSC has a 29% and 29.2% higher annual production. The 2T tandem cell has a 26.5% and 26.8% higher production than the SJC, and the 4T tandem cell annual production is 26.8% and 27.1% higher respectively.

6 Discussion

As seen in figures 17a, 19a, 19b, 19c, 21a, 21c, 21d, 23a, 23c and 23d there are some peaks during the winter, which for some of the cases exceeds the theoretical efficiency limits for the cell concepts. These occurrences are caused by extra cold days with no cloud coverage, this in measured temperature figure 14 and irradiation data figure 15. Also, Lin et al[40] found that increased temperatures contributed significantly to efficiency loss, which inversely relates to the low-temperature effects on the efficiency.

The efficiency plots figures 21b, 23b and 17c has a "layered" shape, that resembles 30. A probable reason for this is the relatively wide band gaps used in these simulations. With band gaps of 1.6 and 2.25/1.55 eV, a significant amount of the incoming photons will not have the energy necessary to excite electrons. Therefore the efficiency increases "stepwise" as the number of high energy photons increases when the airmass spectrum changes. With a smoother transition between the airmass spectra, the efficiency plot could become more fluid.

It appears that having a band gap narrow enough to absorb photons with energies in the 0.8-1.1eV range is desirable, considering figures 17a, 17b, 19a, 19b, 23a, 23c, 23d, 21a, 21c and 21d. This is supported with the findings of G.Kvifte et al[41], where it was found that 43-50% of the solar irradiance is in the 0.44-1.79Ev range.

Comparing the Am1.5 optimal band gaps of IBSC and, 2T and 4T tandem cells, the difference is about 3.6% and 3% higher annual production for the IBSC. Also, comparing the InAs/InGap IBSC with the 2T and 4T Perovskite/CIGS gives a the IBSC about 0.3% better annual production. The Perovskite/Perovskite tandems cells and InAs/GaAs IBSC have a lower performance than the other band gaps for the same concepts, with an annual production of 440 kWh/m^2 for the 2T, 441 kWh/m^2 for the 4T and 453 kWh/m^2 for the IBSC. This gives the IBSC a 2.87% higher production than the 2T and 2.65% better compared to the 4T. This seems to agree with the findings of Naitoh et al[35], which found the IBSC to have about 1% better annual production than 2T triple junction cell. The difference between the annual production of the 4T and 2T at any band gap seems to be in the region of 0.18-0.36%, and this is consistent with findings of Strandberg[12] that the area de-coupled 2T tandem cells can reach the same efficiency as the 4T tandem.

Band gaps used in the simulations was partly chosen based on interest in recent research. These interests are not only based on promising conversion efficiency capabilities but also cost efficiency or other semiconductor material characteristics. This means that there might be band gaps with higher power production capabilities. Furthermore, the band gaps used for the IBSC and tandem cells do not have band gaps with equal photon absorption so that the comparisons might be affected by this.

Even if these simulations use varying cell temperatures and an approximation of spectrum changes, the temperature dependencies of the semiconductor materials are not being taken into account. In a real-world situation, this would affect the performance of the cells. The simulations use Am spectra 1, 1.5, 2, 3, 5 and 10, and this gives an ok representation of the irradiation throughout the day. However, adding additional spectra or calculating the irradiation as a function of the solar position would increase the accuracy of the simulations.

7 Conclusion

Calculations of the power density and efficiencies for the SJC, IBSC, and 2T and 4T tandem cells with four different band gaps have been done, using irradiation and temperature data over a year. The monthly and annual power production for each of the cell concepts has been calculated and compared. Considering the monthly and annual power production of the cells, the IBSC has the highest production if the band gap is optimized for the Am1.5 spectrum. Similarly, for the 2T and 4T tandems cells, band gaps optimized for Am1.5 gives the highest power production. The differences between the IBSC and the 2T and 4T tandem under these conditions are 3% and 3.6% respectively. The IBSC InAs/InGap has been shown to have almost identical annual production as the 2T and 4T Perovskite/CIGS tandem cells, and have a 2.2% and 2% higher production than the 2T and 4T perovskite/Si. The IBSC with band gap Am1.5 has a 29.2% and 29% higher production than SJC with Si and Am1.5 optimized band gap respectively. The tandem cells using am1.5 band gaps have a production that is 26.5% and 26.8% higher than SJC with Am1.5 and Si band gaps.

8 Future work

Continuation of the work done in this thesis could include additional simulations using measured photon flux to better simulate the incoming wavelengths of the locations. Additionally, adding band gap temperature dependencies and other recombination factors could be interesting.

Bibliography

[1] N. Abas, A. Kalair, and N. Khan, "Review of fossil fuels and future energy technologies," *Futures*, vol. 69, pp. 31–49, 2015.

[2] (). Cookie notification, [Online]. Available: https://www.bp.com/en/global/corporate/energy-economics/statistical-review-of-world-energy/renewable-energy/solar-energy.html (visited on 05/16/2018).

[3] W. Shockley and H. J. Queisser, "Detailed balance limit of efficiency of p-n junction solar cells," *Journal of applied physics*, vol. 32, no. 3, pp. 510–519, 1961.

[4] K. Ranabhat, L. Patrikeev, A. Antal'evna-Revina, K. Andrianov, V. Lapshinsky, and E. Sofronova, "An introduction to solar cell technology," *Journal of Applied Engineering Science*, vol. 14, no. 4, pp. 481–491, 2016.

[5] D. R. Myers, *Solar radiation: practical modeling for renewable energy applications*. CRC Press, 2016.

[6] B. Van Zeghbroeck, "Principles of semiconductor devices," *Colarado University*, 2004.

[7] (). Detailed balance, [Online]. Available: http://pveducation.org/pvcdrom/detailed-balance (visited on 04/13/2018).

[8] J. Giesecke, *Quantitative recombination and transport properties in silicon from dynamic luminescence*. Springer, 2014.

[9] J. Nelson, *The physics of solar cells*. World Scientific Publishing Co Inc, 2003.

[10] R. Strandberg, "Analytic *jv*-characteristics of ideal intermediate band solar cells and solar cells with up and downconverters," *IEEE Transactions on Electron Devices*, vol. 64, no. 5, pp. 2275–2282, 2017.

[11] A. Luque, A. Martıó, and C. Stanley, "Understanding intermediate-band solar cells," *Nature Photonics*, vol. 6, no. 3, nphoton–2012, 2012.

[12] R. Strandberg, "Detailed balance analysis of area de-coupled double tandem photovoltaic modules," *Applied Physics Letters*, vol. 106, no. 3, p. 033 902, 2015.

[13] R. Adelhelm and G. La Roche, "Matching of multi junction solar cells for solar array production," in *Photovoltaic Specialists Conference, 2000. Conference Record of the Twenty-Eighth IEEE*, IEEE, 2000, pp. 1336–1339.

[14] S. Bremner, M. Levy, and C. B. Honsberg, "Analysis of tandem solar cell efficiencies under am1. 5g spectrum using a rapid flux calculation method," *Progress in photovoltaics: Research and Applications*, vol. 16, no. 3, pp. 225–233, 2008.

[15] (). Solareqns, National Oceanic and Atmospheric Administration, [Online]. Available: https://www.esrl.noaa.gov/gmd/grad/solcalc/solareqns.PDF (visited on 03/05/2018).

[16] (). Air mass, [Online]. Available: http://www.pveducation.org/pvcdrom/properties-of-sunlight/air-mass (visited on 03/14/2018).

[17] W. E. Sha, X. Ren, L. Chen, and W. C. Choy, "The efficiency limit of ch3nh3pbi3 perovskite solar cells," *Applied Physics Letters*, vol. 106, no. 22, p. 221 104, 2015.

[18] H. S. Jung and N.-G. Park, "Perovskite solar cells: From materials to devices," *small*, vol. 11, no. 1, pp. 10–25, 2015.

[19] K. A. Bush, A. F. Palmstrom, J. Y. Zhengshan, M. Boccard, R. Cheacharoen, J. P. Mailoa, D. P. McMeekin, R. L. Hoye, C. D. Bailie, T. Leijtens, *et al.*, "23.6%-efficient monolithic perovskite/silicon tandem solar cells with improved stability," *Nature Energy*, vol. 2, no. 4, p. 17 009, 2017.

[20] (). Semiconductor band gaps, Georgia State Univeristy, [Online]. Available: http://hyperphysics.phy-astr.gsu.edu/hbase/Solids/bandgap.html (visited on 04/10/2018).

[21] E. Yablonovitch, O. D. Miller, and S. Kurtz, "The opto-electronic physics that broke the efficiency limit in solar cells," in *Photovoltaic Specialists Conference (PVSC), 2012 38th IEEE*, IEEE, 2012, pp. 001 556–001 559.

[22] T. Wilkins. (). Why use gallium arsenide solar cells? [Online]. Available: https://www.altadevices.com/use-gallium-arsenide-solar-cells/ (visited on 04/17/2018).

[23] J. H. Heo and S. H. Im, "Ch3nh3pbbr3–ch3nh3pbi3 perovskite–perovskite tandem solar cells with exceeding 2.2 v open circuit voltage," *Advanced Materials*, vol. 28, no. 25, pp. 5121–5125, 2016.

[24] P. Mantilla-Perez, T. Feurer, J.-P. Correa-Baena, Q. Liu, S. Colodrero, J. Toudert, M. Saliba, S. Buecheler, A. Hagfeldt, A. N. Tiwari, *et al.*, "Monolithic cigs–perovskite tandem cell for optimal light harvesting without current matching," *ACS photonics*, vol. 4, no. 4, pp. 861–867, 2017.

[25] K. Xiong, H. Mi, T.-H. Chang, D. Liu, Z. Xia, M.-Y. Wu, X. Yin, S. Gong, W. Zhou, J. C. Shin, *et al.*, "Algaas/si dual-junction tandem solar cells by epitaxial lift-off and print-transfer-assisted direct bonding," *Energy Science & Engineering*, 2018.

[26] A. De Vos, "Detailed balance limit of the efficiency of tandem solar cells," *Journal of Physics D: Applied Physics*, vol. 13, no. 5, p. 839, 1980.

[27] T. Duong, Y. Wu, H. Shen, J. Peng, X. Fu, D. Jacobs, E.-C. Wang, T. C. Kho, K. C. Fong, M. Stocks, *et al.*, "Rubidium multication perovskite with optimized bandgap for perovskite-silicon tandem with over 26% efficiency," *Advanced Energy materials*, vol. 7, no. 14, 2017.

[28] R. S. Ohl, *Light-sensitive electric device*, US Patent 2,402,662, Jun. 1946.

[29] B. M. Kayes, H. Nie, R. Twist, S. G. Spruytte, F. Reinhardt, I. C. Kizilyalli, and G. S. Higashi, "27.6% conversion efficiency, a new record for single-junction solar cells under 1 sun illumination," in *Photovoltaic Specialists Conference (PVSC), 2011 37th IEEE*, IEEE, 2011, pp. 000 004–000 008.

[30] Y. Okada, N. Ekins-Daukes, T. Kita, R. Tamaki, M. Yoshida, A. Pusch, O. Hess, C. Phillips, D. Farrell, K. Yoshida, *et al.*, "Intermediate band solar cells: Recent progress and future directions," *Applied physics reviews*, vol. 2, no. 2, p. 021 302, 2015.

[31] A. Martıó, L. Cuadra, and A. Luque, "Quantum dot intermediate band solar cell," in *Photovoltaic Specialists Conference, 2000. Conference Record of the Twenty-Eighth IEEE*, IEEE, 2000, pp. 940–943.

[32] W. Shan, W. Walukiewicz, J. Ager III, E. Haller, J. Geisz, D. Friedman, J. Olson, and S. R. Kurtz, "Band anticrossing in gainnas alloys," *Physical Review Letters*, vol. 82, no. 6, p. 1221, 1999.

[33] A. Luque, A. Martıó, E. Antolıón, and C. Tablero, "Intermediate bands versus levels in non-radiative recombination," *Physica B: Condensed Matter*, vol. 382, no. 1-2, pp. 320–327, 2006.

[34] M. Yoshida, N. Ekins-Daukes, D. Farrell, and C. Phillips, "Photon ratchet intermediate band solar cells," *Applied Physics Letters*, vol. 100, no. 26, p. 263 902, 2012.

[35] S. Naitoh and Y. Okada, "Efficiency estimations for multijunction and intermediate band solar cells using actual measured solar spectra in japan," *Journal of Solar Energy Engineering*, vol. 137, no. 3, p. 034 504, 2015.

[36] A. S. Brown and M. A. Green, "Limiting efficiency for current-constrained two-terminal tandem cell stacks," *Progress in photovoltaics: Research and Applications*, vol. 10, no. 5, pp. 299–307, 2002.

[37] N. Jain, K. L. Schulte, J. F. Geisz, D. J. Friedman, R. M. France, E. E. Perl, A. G. Norman, H. L. Guthrey, and M. A. Steiner, "High-efficiency inverted metamorphic 1.7/1.1 ev gainasp/gainas dual-junction solar cells," *Applied Physics Letters*, vol. 112, no. 5, p. 053 905, 2018.

[38] O. Dupré, B. Niesen, S. De Wolf, and C. Ballif, "Field performance versus standard test condition efficiency of tandem solar cells and the specific case of perovskites/silicon devices," *The journal of physical chemistry letters*, 2018.

[39] M. Schweiger, W. Herrmann, A. Gerber, and U. Rau, "Understanding the energy yield of photovoltaic modules in different climates by linear performance loss analysis of the module performance ratio," *IET Renewable Power Generation*, vol. 11, no. 5, pp. 558–565, 2017.

[40] H. Liu, Z. Ren, Z. Liu, A. G. Aberle, T. Buonassisi, and I. M. Peters, "Predicting the outdoor performance of flat-plate iii–v/si tandem solar cells," *Solar Energy*, vol. 149, pp. 77–84, 2017.

[41] G. Kvifte, K. Hegg, and V. Hansen, "Spectral distribution of solar radiation in the nordic countries," *Journal of climate and applied meteorology*, vol. 22, no. 1, pp. 143–152, 1983.

Appendix A 2T top/bottom cell combinations

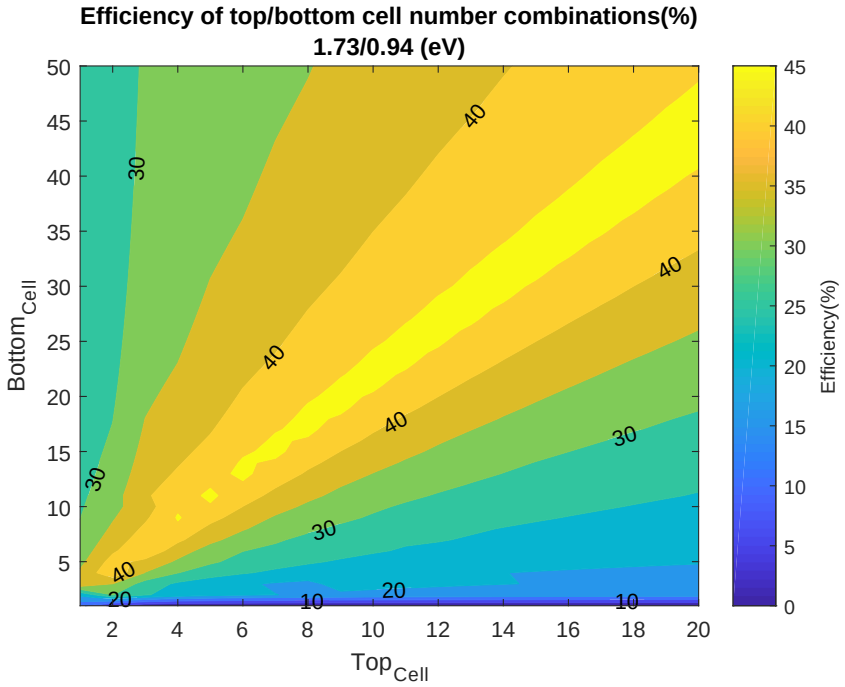

Figure 26: Simulation results showing the efficiency of the 2T tandem cell with different number of bottom and top cells, for 1.73/0.94eV bandgap

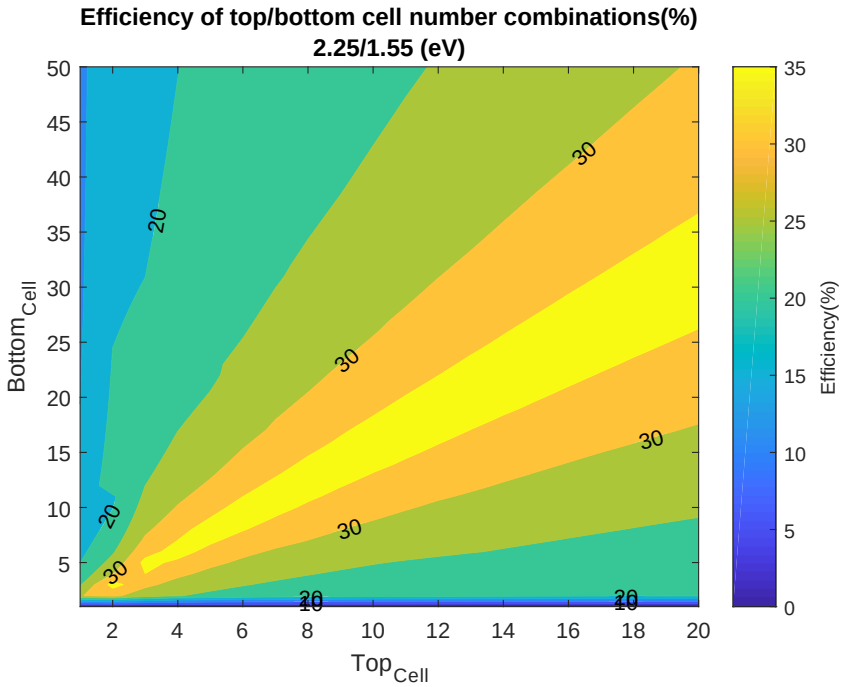

Figure 27: Simulation results showing the efficiency of the 2T tandem cell with different number of bottom and top cells, for 2.25/1.55eV bandgap

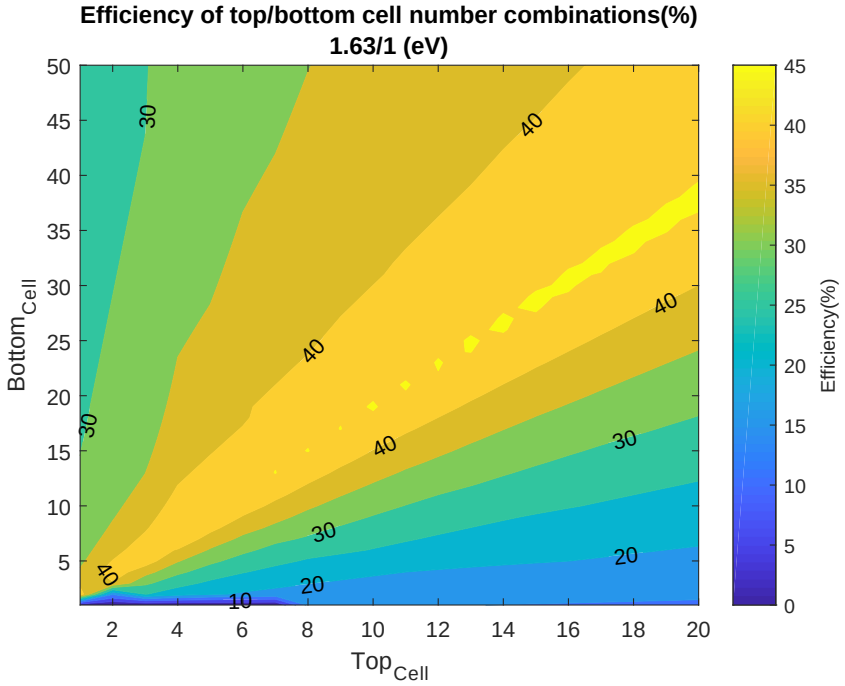

Figure 28: Simulation results showing the efficiency of the 2T tandem cell with different number of bottom and top cells, for 1.63/1eV bandgap

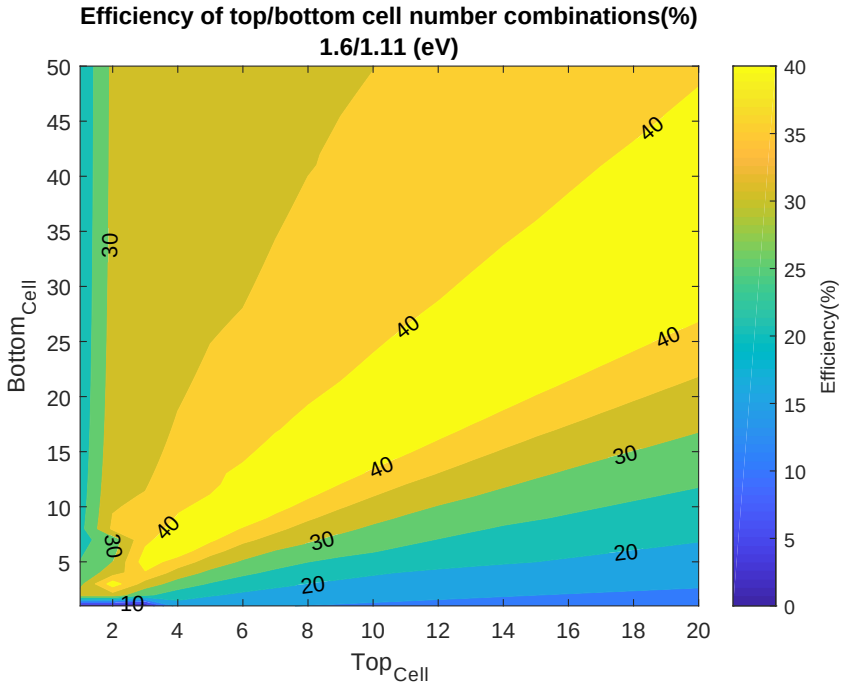

Figure 29: Simulation results showing the efficiency of the 2T tandem cell with different number of bottom and top cells, for 1.6/1.11eV bandgap

Appendix B Am distribution

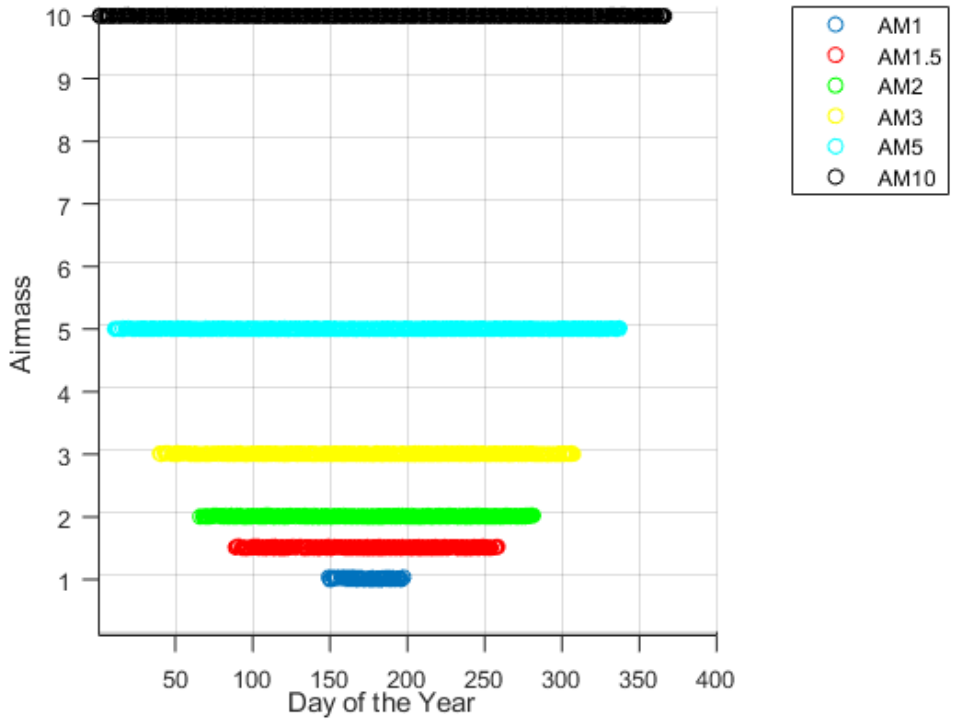

Figure 30: Shows how the distribution of the airmass throughout the year used in the simulation

Appendix C MatLab scripts

Appendix D MatLab Solar position

```
%function that calculates the sun position on the sky, based on day of the
%year, hours, minutes and seconds. Returns the airmass that corresponds to
%the position of the sun and the temperature and irradiation measured at
%the given time. Ignores values during night time.
function [Z,Temp,Airmass,dager,dagdag,TII] = Solposisjon(filnavn)

L =1;
data=importdata([filnavn,'.csv']);
Tempa = data.data(:,27);
month = data.data(:,2);
dag = data.data(:,3);
time = data.data(:,4);
minutt = data.data(:,5);
sekund = data.data(:,6);
skraaplanstraaling = data.data(:,10); % Tilted irradiation
long = 8.59343;
lat = 58.3405;
timezone = 1;
k =1;

for i =1:15:length(dag)
hour =time(i);
min = minutt(i);
sec = sekund(i);
d = dag(i);
m =month(i);
y = 2016;
date1= string([y,m,d]);
Date= join(date1,'-');
dd= datetime(Date,'InputFormat','yyyy-MM-dd');
doy=day(dd,'dayofyear');
dagdagdag(i)= doy;
yoy= (2*pi/365)*((doy-1)+((hour-12)/24));
eot= 229.18*(0.000075+0.001868*cos(yoy)-0.032077*sin(yoy)-0.014615*cos(2*
    yoy)-0.040849*sin(2*yoy));
decl= 0.006918-0.399912*cos(yoy)+0.070257*sin(yoy)-0.006758*cos(2*yoy)
    +0.000907*sin(2*yoy)-0.002697*cos(3*yoy)+0.00148*sin(3*yoy);
timeoffset= eot+(4*long)-(60*timezone);
tst= (hour*60)+min+(sec/60)+timeoffset;
HA= (tst/4)-180;
Z= acosd((sind(lat)*sin(decl))+(cosd(lat)*cos(decl)*cosd(HA)));
Am(i) = 1/cosd(Z);
%sorts the results into whats usefull or not%
if Am(i) < 0
Airmass(k)=NaN;
dager(k) = NaN;
```

```
Temp(k) = NaN;
dagdag(k) = NaN;
TII(k) = NaN;
elseif Am(i) > 15
Airmass(k)=NaN;
dager(k)=NaN;
Temp(k) = NaN;
dagdag(k) = NaN;
TII(k) = NaN;
else
Airmass(k)=Am(i);
dager(k)=dag(i);
Temp(k)=Tempa(i);
dagdag(k) = dagdagdag(i);
TII(k) = skraaplanstraaling(i);
end
k=k+1;
end
%Removes unwanted values%
Temp = Temp(~isnan(Temp));
Airmass = Airmass(~isnan(Airmass));
dager = dager(~isnan(dager));
dagdag=dagdag(~isnan(dagdag));
TII = TII(~isnan(TII));
```

Appendix E MatLab Single Junction Solar Cell

```
% calculates the power denisty and efficiencies for the single junction
    cell
% with four different band gaps and based on the data returned
% by functions Solposisjon.m and GetSpectrum.m
close all;
clear all;
clc;
%-------------------------------------------------------------------%
%Declaring the constants. Defining and sizing the variables%
%-------------------------------------------------------------------%
k = 1.38064852e-23;
q = 1.6022176e-19;
h = 6.626176e-34;
c = 299792458;
E = 6;


Eq = E*q;
fun = 0;
Const = (2*pi)/(h^3*c^2);
tid = 1;

ebg= [1.34 1.11 1.6 1.424];


%
    ------------------------------------------------------------------------


%Calling functions "Solposisjon" which returns airmass variations(Airmass)
    ,                                   %
%temperature(Temp) for each day and measured irradiance(TII), and "
    GetSpectrum" which returns the number of%
%photons, photon energy and irradiance for airmass 1,1.5,2,3,5 and 10.
                                        %
%
    ------------------------------------------------------------------------


[E_AM1,E_AM15,E_AM2,E_AM3,E_AM5,E_AM10,AM1fotoner,AM15fotoner,AM2fotoner,
    AM3fotoner,AM5fotoner,AM10fotoner,AM1innenergi,AM15innenergi,
    AM2innenergi,AM3innenergi, AM5innenergi,AM10innenergi]=GetSpectrum();
[Z,Temp,Airmass,dager,dagdag,TII] = Solposisjon('combined2016');
%Presets the array sizes
Am = zeros(length(Airmass),6);
Ptotal=zeros(4,length(Airmass));
Eff=zeros(4,length(Airmass));
volt=zeros(4,length(Airmass));
current=zeros(4,length(Airmass));
day =zeros(1,length(Airmass));
```

```
for j=1:1:length(ebg)
Et = ebg(j);
Etopq = Et*q;
%-------------------------------------------------------------------------%
%Determines the current airmass and gives the variables theappropriate  %
%values to be used in the calculations                                   %
%-------------------------------------------------------------------------%
for i=1:1:length(Airmass)
if (1<= Airmass(i)) && (Airmass(i) <1.25)
Spekter = AM1fotoner*(TII(i)/AM1innenergi);
Etot = E_AM1;
P = AM1innenergi*(TII(i)/AM1innenergi);
Am(i,1)= 1;
elseif (1.25 <= Airmass(i)) && (Airmass(i)<1.75)
Spekter = AM15fotoner*(TII(i)/AM15innenergi);
Etot = E_AM15;
P = AM15innenergi*(TII(i)/AM15innenergi);
Am(i,2)= 1.5;
elseif (1.75<= Airmass(i)) && (Airmass(i)<2.30)
Spekter = AM2fotoner*(TII(i)/AM2innenergi);
Etot = E_AM2;
P = AM2innenergi*(TII(i)/AM2innenergi);
Am(i,3)= 2;
elseif (2.30<= Airmass(i)) && (Airmass(i)<3.50)
Spekter = AM3fotoner*(TII(i)/AM3innenergi);
Etot = E_AM3;
P = AM3innenergi*(TII(i)/AM3innenergi);
Am(i,4)= 3;
elseif (3.50<= Airmass(i)) && (Airmass(i)<=6)
Spekter = AM5fotoner*(TII(i)/AM5innenergi);
Etot = E_AM5;
P = AM5innenergi*(TII(i)/AM5innenergi);
Am(i,5)= 5;
elseif (6< Airmass(i)) && (Airmass(i)<16)
Spekter = AM10fotoner*(TII(i)/AM10innenergi);
Etot = E_AM10;
P = AM10innenergi*(TII(i)/AM10innenergi);
Am(i,6)= 10;
end

day(i) = dagdag(i);
T = Temp(i)+273.15;
Gtop = 0;
for k1=1:1:length(Spekter)      %Estimating the photon generation%
if Etot(k1) > Et              %rate in the bandgap              %
Gtop = Gtop+Spekter(k1);
end
end
%-------------------------------------------------------------------------%
```

```
%Calculating recombination, Vmpp and Pmpp                    %
%-------------------------------------------------------------%
fun = @(x,v) exp((q*v-x)./(k*T)).*x.^2;
fun2 = @(v) v*q*(Gtop-Const*(integral(@(x)fun(x,v),Etopq,Eq)));
v0 = 1;
options = optimoptions(@fminunc,'Display','none','OptimalityTolerance',1e
    -40);
[v,fval] = fminunc(@(v)-fun2(v),v0,options);
Po1 = -fval;
Ptotal(j,i) = Po1;
Eff(j,i) = (Ptotal(j,i)/P)*100;
volt(j,i) = v;
current(j,i) = Po1/v;
hvaskjer=hvaskjer+1
end
end
```

Appendix F MatLab Intermediate band solar cell

```
% calculates the power denisty and efficiencies for the intermediate band
% solar cell, with four different band gaps and based on the data returned
% by functions Solposisjon.m and GetSpectrum.m
clear all;
close all;
clc;
%Defines constants and variables
k = 1.38064852e-23;
q = 1.6022176e-19;
h = 6.626176e-34;
c = 299792458;
T = 298.15;
E = 6;
Eq = E*q;

Const = ((2*pi)/(h^3*c^2));

Ecv = [1.95 1.88 1.424 2];
Eiv = [1.24 1.26 1.07 1.424];
Eci = [0.71 0.62 0.354 0.576];
%-------------------------------------------------------------------------

%Calling functions "Solposisjon" which returns airmass variations(Airmass),                                    %
%temperature(Temp) for each day and measured irradiance(TII), and "GetSpectrum" which returns the number of%
%photons, photon energy and irradiance for airmass 1,1.5,2,3,5 and 10.                                          %
%-------------------------------------------------------------------------

[E_AM1,E_AM15,E_AM2,E_AM3,E_AM5,E_AM10,AM1fotoner,AM15fotoner,AM2fotoner,AM3fotoner,AM5fotoner,AM10fotoner,AM1innenergi,AM15innenergi,AM2innenergi,AM3innenergi, AM5innenergi,AM10innenergi]=GetSpectrum();
[Z,Temp,Airmass,dager,dagdag,TII] = Solposisjon('combined2016');
%preset the array size
Ptotal=NaN(4,length(Airmass));
Eff=NaN(4,length(Airmass));
for j=1:1:length(Ecv)
ecv = Ecv(j);
eiv = Eiv(j);
eci = Eci(j);
for i=1:1:length(Airmass)
%-------------------------------------------------------------------------%
%Determines the current airmass and gives the variables theappropriate  %
%values to be used in the calculations                                    %
%-------------------------------------------------------------------------%
```

```
if (1<= Airmass(i)) && (Airmass(i) <1.25)
Spekter = AM1fotoner*(TII(i)/AM1innenergi);
Egap= E_AM1;
Etot = E_AM1;
P = AM1innenergi*(TII(i)/AM1innenergi);

elseif (1.25 <= Airmass(i)) && (Airmass(i)<1.75)
Spekter = AM15fotoner*(TII(i)/AM15innenergi);
Etot = E_AM15;
P = AM15innenergi*(TII(i)/AM15innenergi);

elseif (1.75<= Airmass(i)) && (Airmass(i)<2.30)
Spekter = AM2fotoner*(TII(i)/AM2innenergi);
Etot = E_AM2;
P = AM2innenergi*(TII(i)/AM2innenergi);

elseif (2.30<= Airmass(i)) && (Airmass(i)<3.50)
Spekter = AM3fotoner*(TII(i)/AM3innenergi);
Etot = E_AM3;
P = AM3innenergi*(TII(i)/AM3innenergi);

elseif (3.50<= Airmass(i)) && (Airmass(i)<=6)
Spekter = AM5fotoner*(TII(i)/AM5innenergi);
Etot = E_AM5;
P = AM5innenergi*(TII(i)/AM5innenergi);

elseif (6< Airmass(i)) && (Airmass(i)<16)
Spekter = AM10fotoner*(TII(i)/AM10innenergi);
Etot = E_AM10;
P = AM10innenergi*(TII(i)/AM10innenergi);

end
gci = 0;
gcv = 0;
giv = 0;
%determines the number of photons
for i2=1:1:length(Spekter)
if Etot(i2)>eci && Etot(i2) < eiv
gci = gci+Spekter(i2);
elseif Etot(i2) > eiv && Etot(i2)< ecv
giv = giv+Spekter(i2);
elseif Etot(i2) > ecv && Etot(i2) < 5
gcv = gcv+Spekter(i2);
end
end
ecvq = ecv*q;
eivq = eiv*q;
eciq = eci*q;
T = Temp(i)+273.15;
```

```
89  fun = @(x) exp((-x)./(k*T)).*x.^2;
90  funeiv = integral(fun,eivq,ecvq);
91  funeci = integral(fun,eciq,eivq);
92  funecv = integral(fun,ecvq,E*q);
93
94  R0ci=funeci*Const;%recombination parameters
95  R0iv=funeiv*Const;
96  R0cv=funecv*Const;
97
98  optifun = @(v) q*v*(gcv+(0.5*(gci+giv))-(R0cv.*exp(q*v./(k*T)))-(0.5.*sqrt
        ((4.*R0ci.*R0iv).*exp(q*v./(k*T))+(gci-giv).^2)));
99  v0 = 0.1;
100 options = optimoptions(@fminunc,'Display','none','OptimalityTolerance',1e
        -5);
101 %calculates Pmpp and Vmpp
102 [v,fval] = fminunc(@(v)-optifun(v),v0,options);
103 Ptot=-fval;
104 Ptotal(j,i)=Ptot;
105 Eff(j,i) = (Ptot/P)*100;
106 end
107 end
```

Appendix G MatLab 4 terminal tandem cell

```
% calculates the power denisty and efficiencies for the 4 terminal tandem cell,
% with four different band gaps and based on the data returned
% by functions Solposisjon.m and GetSpectrum.m
close all;
clear all;
clc;
%defines variables and constants
k = 1.38064852e-23;
q = 1.6022176e-19;
h = 6.626176e-34;
c = 3e+8;
R = 0.1;
T = 300;
E = 4.5;
Eq = E*q;
fun = 0;
Const = (2*pi)/(h^3*c^2);
tid = 1;

et= [1.73 2.25 1.63 1.6];
eb= [0.94 1.55 1 1.11];

Ptotal=zeros(4,12e+3);
Eff=zeros(4,12e+3);

day =zeros(1,12e+3);
%-------------------------------------------------------------------------

%Calling functions "Solposisjon" which returns airmass variations(Airmass),                                    %
%temperature(Temp) for each day and measured irradiance(TII), and "GetSpectrum" which returns the number of%
%photons, photon energy and irradiance for airmass 1,1.5,2,3,5 and 10.                                          %
%-------------------------------------------------------------------------


[E_AM1,E_AM15,E_AM2,E_AM3,E_AM5,E_AM10,AM1fotoner,AM15fotoner,AM2fotoner,AM3fotoner,AM5fotoner,AM10fotoner,AM1innenergi,AM15innenergi,AM2innenergi,AM3innenergi, AM5innenergi,AM10innenergi]=GetSpectrum();
[Z,Temp,Airmass,dager,dagdag,TII] = Solposisjon('combined2016');
%presets array sizes
Am = zeros(length(Airmass),6);
volt2= NaN(4,12e+3);
volt1= NaN(4,12e+3);
```

```
gbottom= NaN(4,12e+3);
gtop= NaN(4,12e+3);
pp= NaN(4,12e+3);
div= NaN(4,12e+3);
gtotal=NaN(4,12e+3);
for j=1:1:length(et)
Et = et(j);
Eb = eb(j);
Etopq = Et*q;
Ebq = Eb*q;
for i=1:1:length(Airmass)
%-------------------------------------------------------------------------%
%Determines the current airmass and gives the variables theappropriate  %
%values to be used in the calculations                                   %
%-------------------------------------------------------------------------%
if (1<= Airmass(i)) && (Airmass(i) <1.25)
Spekter = AM1fotoner*(TII(i)/AM1innenergi);
Egap= E_AM1;
Etot = E_AM1;
P = AM1innenergi*(TII(i)/AM1innenergi);
pp(j,i) = AM1innenergi*(TII(i)/AM1innenergi);
Am(i,1)= 1;

elseif (1.25 <= Airmass(i)) && (Airmass(i)<1.75)
Spekter = AM15fotoner*(TII(i)/AM15innenergi);
Etot = E_AM15;
P = AM15innenergi*(TII(i)/AM15innenergi);
pp(j,i) = AM15innenergi*(TII(i)/AM15innenergi);
Am(i,2)= 1.5;
elseif (1.75<= Airmass(i)) && (Airmass(i)<2.30)
Spekter = AM2fotoner*(TII(i)/AM2innenergi);
Etot = E_AM2;
P = AM2innenergi*(TII(i)/AM2innenergi);
pp(j,i) = AM2innenergi*(TII(i)/AM2innenergi);
Am(i,3)= 2;
elseif (2.30<= Airmass(i)) && (Airmass(i)<3.50)
Spekter = AM3fotoner*(TII(i)/AM3innenergi);
Etot = E_AM3;
P = AM3innenergi*(TII(i)/AM3innenergi);
pp(j,i) = AM3innenergi*(TII(i)/AM3innenergi);
Am(i,4)= 3;
elseif (3.50<= Airmass(i)) && (Airmass(i)<=6)
Spekter = AM5fotoner*(TII(i)/AM5innenergi);
Etot = E_AM5;
P = AM5innenergi*(TII(i)/AM5innenergi);
pp(j,i) = AM5innenergi*(TII(i)/AM5innenergi);
Am(i,5)= 5;
elseif (6< Airmass(i)) && (Airmass(i)<16)
Spekter = AM10fotoner*(TII(i)/AM10innenergi);
```

```
88  Etot = E_AM10;
89  P = AM10innenergi*(TII(i)/AM10innenergi);
90  pp(j,i) = AM10innenergi*(TII(i)/AM10innenergi);
91  Am(i,6)= 10;
92  end
93
94  day(i) = dagdag(i);
95  T = Temp(i)+273.15;
96  Gtop = 0;
97  %number of photons to the top cell
98  for k1=1:1:length(Spekter)
99  if Etot(k1) > Et
100 Gtop = Gtop+Spekter(k1);
101 end
102 end
103
104 fun = @(x,v) exp((q*v-x)./(k*T)).*x.^2;
105 fun2 = @(v) v*q*(Gtop-Const*(integral(@(x)fun(x,v),Etopq,Eq)));
106 v0 = 1;
107 options = optimoptions(@fminunc,'Display','none','OptimalityTolerance',1e
        -40);
108 [v,fval] = fminunc(@(v)-fun2(v),v0,options);
109 Po1 = -fval;
110 volt1(j,i) =v;
111 Gb = 0;
112 %number of photons to the bottom cell
113 for k2=1:1:length(Spekter)
114 if Etot(k2) > Eb && Etot(k2) < Et
115 Gb = Gb+Spekter(k2);
116 end
117 end
118 gbottom(j,i)=Gb;
119 gtop(j,i)=Gtop;
120 funktion = @(x1,v2) exp((q*v2-x1)./(k*T)).*x1.^2;
121 funktion2 = @(v2) v2*q*(Gb-Const*(integral(@(x1)funktion(x1,v2),Ebq,Etopq)
        ));
122 v20 = 1;
123 options1 = optimoptions(@fminunc,'Display','none','OptimalityTolerance',1e
        -40);
124 [v2,fv2al] = fminunc(@(v2)-funktion2(v2),v20,options1);
125 %calculates Pmpp and Vmpp
126 Po2 = -fv2al;
127 Ptotal(j,i) = Po1+Po2;
128 Eff(j,i) = (Ptotal(j,i)/P)*100;
129 volt2(j,i)= v2;
130
131 end
132 end
```

Appendix H MatLab 2 terminal tandem cell

```
% calculates the power denisty and efficiencies for the 2 terminal area
% de-coupled tandem cell,
% with four different band gaps and based on the data returned
% by functions Solposisjon.m and GetSpectrum.m
close all;
clear all;
clc;
format long g;
k = 1.38064852e-23;
q = 1.6022176e-19;
h = 6.626176e-34;
c = 299792458;
T = 300;
E = 6;
Eq = E*q;
dettetartid = 1;
Const = ((2*pi)/(h^3*c^2));

et= [1.73 2.25 1.63 1.6];
eb= [0.94 1.55 1 1.11];
mt = [1 1 1 1];
nb = [2.2 1.55 1.88 1.625];
%
    ------------------------------------------------------------------------------------------

%Calling functions "Solposisjon" which returns airmass variations(Airmass),                %
%temperature(Temp) for each day and measured irradiance(TII), and "GetSpectrum" which returns the number of%
%photons, photon energy and irradiance for airmass 1,1.5,2,3,5 and 10.                      %
%
    ------------------------------------------------------------------------------------------

[E_AM1,E_AM15,E_AM2,E_AM3,E_AM5,E_AM10,AM1fotoner,AM15fotoner,AM2fotoner,AM3fotoner,AM5fotoner,AM10fotoner,AM1innenergi,AM15innenergi,AM2innenergi,AM3innenergi, AM5innenergi,AM10innenergi]=GetSpectrum();
[Z,Temp,Airmass,dager,dagdag,TII] = Solposisjon('combined2016');
%presets the array size
Ptotal=NaN(4,length(Airmass));
Eff=NaN(4,length(Airmass));
vtot=NaN(4,length(Airmass),300);
Am=NaN(length(Airmass),6);
dust=0;
for j = 1:1:length(et)
m=mt(j);
n=nb(j);
for i=1:1:length(Airmass)
```

```
if (1<= Airmass(i)) && (Airmass(i) <1.25)
Spekter = AM1fotoner*(TII(i)/AM1innenergi);
Etot = E_AM1;
P = AM1innenergi*(TII(i)/AM1innenergi);
Am(i,1)= 1;
elseif (1.25 <= Airmass(i)) && (Airmass(i)<1.75)
Spekter = AM15fotoner*(TII(i)/AM15innenergi);
Etot = E_AM15;
P = AM15innenergi*(TII(i)/AM15innenergi);
Am(i,2)= 1.5;
elseif (1.75<= Airmass(i)) && (Airmass(i)<2.30)
Spekter = AM2fotoner*(TII(i)/AM2innenergi);
Etot = E_AM2;
P = AM2innenergi*(TII(i)/AM2innenergi);
Am(i,3)= 2;
elseif (2.30<= Airmass(i)) && (Airmass(i)<3.50)
Spekter = AM3fotoner*(TII(i)/AM3innenergi);
Etot = E_AM3;
P = AM3innenergi*(TII(i)/AM3innenergi);
Am(i,4)= 3;
elseif (3.50<= Airmass(i)) && (Airmass(i)<=6)
Spekter = AM5fotoner*(TII(i)/AM5innenergi);
Etot = E_AM5;
P = AM5innenergi*(TII(i)/AM5innenergi);
Am(i,5)= 5;
elseif (6< Airmass(i)) && (Airmass(i)<16)
Spekter = AM10fotoner*(TII(i)/AM10innenergi);
Etot = E_AM10;
P = AM10innenergi*(TII(i)/AM10innenergi);
Am(i,6)= 10;
end
Et=et(j);
Eb=eb(j);
T = Temp(i)+273.15;
Gtop =0;
Gb =0;
%determines number of photons
for i2 =1:1:length(Spekter)
if Etot(i2)>=Et
Gtop=Gtop+Spekter(i2);
end
end
for k1 = 1:1:length(Spekter)
if Etot(k1) >= Eb && Etot(k1)< Et
Gb = Gb+Spekter(k1);
end
end
Etopq = Et*q;
Ebq= Eb*q;
```

```
Ptot = 0;
Ptemp = 0;
v = 0;
c1=1;
Pare = NaN(1,300);

while Ptot >= Ptemp
v = v+0.01;
Ptemp = Ptot;

funtop = @(x1) exp((q*v/m-x1)./(k*T)).*x1.^2;
funbunn = @(x2) exp((q*v/n-x2)./(k*T)).*x2.^2;
%calculates top and bottom cell currents
Itop = (q*(Gtop-Const*(integral(@(x1)funtop(x1),Etopq,Eq))))/m;
Ibunn=(q*(Gb-Const*(integral(@(x2)funbunn(x2),Ebq,Etopq))))/n;

Ptot = v*(Itop+Ibunn);
Pare(c1)= Ptot;
vtot(j,i,c1) = v;
c1 = c1+1;
end
Ptotal(j,i)=Ptot;
Eff(j,i)=max(Pare)/P*100;

end
end
```

Appendix I MatLab Spectra

```
%This function returns data collected from the standardized airmass
%spectra, 1,1.5,2,3,5 and 10.
function [E_AM1,E_AM15,E_AM2,E_AM3,E_AM5,E_AM10,AM1fotoner,AM15fotoner,
    AM2fotoner,AM3fotoner,AM5fotoner,AM10fotoner,AM1innenergi,
    AM15innenergi,AM2innenergi,AM3innenergi, AM5innenergi,AM10innenergi]=
    GetSpectrum()



Am1=importdata(['AM1','.csv']);
E_AM1=Am1.data(:,1);
AM1energi=Am1.data(:,2);
AM1fotoner=Am1.data(:,3);
AM1innenergi=sum(AM1energi);

Am15=importdata(['AM15','.csv']);
E_AM15=Am15.data(:,1);
AM15energi=Am15.data(:,2);
AM15fotoner=Am15.data(:,3);
AM15innenergi=sum(AM15energi);

Am2=importdata(['AM2','.csv']);
E_AM2=Am2.data(:,1);
AM2energi=Am2.data(:,2);
AM2fotoner=Am2.data(:,3);
AM2innenergi=sum(AM2energi);

Am3=importdata(['AM3','.csv']);
E_AM3=Am3.data(:,1);
AM3energi=Am3.data(:,2);
AM3fotoner=Am3.data(:,3);
AM3innenergi=sum(AM3energi);

Am5=importdata(['AM5','.csv']);
E_AM5=Am5.data(:,1);
AM5energi=Am5.data(:,2);
AM5fotoner=Am5.data(:,3);
AM5innenergi=sum(AM5energi);

Am10=importdata(['AM10','.csv']);
E_AM10=Am10.data(:,1);
AM10energi=Am10.data(:,2);
AM10fotoner=Am10.data(:,3);
AM10innenergi=sum(AM10energi);
end
```

Table 2: Monthly production for the SJCs and IBSCs

	SJC Am1.5 optimal (kWh/m^2)	SJC Si (kWh/m^2)	SJC Perovskite (kWh/m^2)	SJC GaAs (kWh/m^2)	IBSC Am1.5 optimal (kWh/m^2)	IBSC InAs/InGap (kWh/m^2)	IBSC InAs/GaAs (kWh/m^2)	IBSC AlGaAs/GaAs (kWh/m^2)
Jan	18.062	18.87	14.479	17.274	26.074	24.399	21.027	22.684
Feb	30.423	30.639	26.183	29.557	43.107	40.949	34.207	38.727
Mar	39.049	38.778	34.637	38.187	55.037	52.627	43.498	50.053
April	45.852	45.377	40.965	44.912	64.519	61.788	50.921	58.853
May	41.819	41.234	37.558	41.018	58.59	56.154	46.015	53.599
June	41.531	40.849	37.465	40.779	58.065	55.703	45.521	53.239
July	36.899	36.311	33.249	36.222	51.591	49.471	40.422	47.268
Aug	39.591	39.032	35.516	38.826	55.373	53.044	43.383	50.647
Sep	39.601	39.129	35.377	38.799	55.47	53.097	43.535	50.649
Oct	37.043	36.778	32.725	36.207	51.946	49.604	40.799	47.237
Nov	22.612	22.811	19.361	21.946	32.006	30.356	25.328	28.691
Dec	15.715	16.85	11.963	14.865	22.91	21.233	18.674	19.512
Annual	408.197	406.658	359.478	398.592	574.688	548.425	453.33	521.159

Table 3: Monthly production for the 2 terminal and 4 terminal tandem cells

	4T tandem Am1.5 optimal (kWh/m^2)	4T tandem Perovskite/Perovskite (kWh/m^2)	4T tandem Perovskite/CIGS (kWh/m^2)	4T tandem Perovskite/Si (kWh/m^2)	2T tandem Am1.5 optimal (kWh/m^2)	2T tandem Perovskite/Perovskite (kWh/m^2)	2T tandem Perovskite/CIGS (kWh/m^2)	2T tandem Perovskite/Si (kWh/m^2)
Jan	24.796	17.572	24.521	24.077	24.733	17.546	24.462	24.012
Feb	41.507	31.987	40.923	40.102	41.432	31.936	40.822	40.021
Mar	53.293	42.51	52.446	51.303	53.19	42.437	52.312	51.206
April	62.587	50.341	61.569	60.202	62.473	50.25	61.409	60.094
May	57.05	46.216	56.127	54.891	56.916	46.117	55.948	54.78
June	56.651	46.167	55.725	54.494	56.515	46.064	55.529	54.386
July	50.334	40.964	49.517	48.427	50.201	40.87	49.339	48.33
Aug	53.99	43.702	53.132	51.981	53.846	43.6	52.94	51.874
Sep	54.003	43.495	53.154	52.01	53.87	43.402	52.974	51.903
Oct	50.482	40.158	49.726	48.697	50.355	40.072	49.553	48.602
Nov	30.838	23.644	30.424	29.832	30.765	23.602	30.333	29.77
Dec	21.719	14.492	21.517	21.154	21.668	14.472	21.465	21.097
Annual	557.25	441.248	548.781	537.17	555.964	440.368	547.086	536.075